






REVIEW ARTICLE | JUNE 15 2023

Photothermal strategies for ice accretion prevention and ice removal

Tongtong Hao ; Dan Wang; Xiaoting Chen; Abdullatif Jazzar ; Pengju Shi ; Cunyi Li ; Heran Wang; Ximin He  ; Zhiyuan He  



Applied Physics Reviews 10, 021317 (2023)

<https://doi.org/10.1063/5.0148288>



CrossMark

AIP Advances

Why Publish With Us?

-  **25 DAYS**
average time to 1st decision
-  **740+ DOWNLOADS**
average per article
-  **INCLUSIVE**
scope

[Learn More](#)



Photothermal strategies for ice accretion prevention and ice removal



Cite as: Appl. Phys. Rev. **10**, 021317 (2023); doi: [10.1063/5.0148288](https://doi.org/10.1063/5.0148288)

Submitted: 28 February 2023 · Accepted: 8 May 2023 ·

Published Online: 15 June 2023



View Online



Export Citation



CrossMark

Tongtong Hao,¹ Dan Wang,¹ Xiaoting Chen,¹ Abdullatif Jazzar,² Pengju Shi,² Cunyi Li,³ Heran Wang,⁴ Ximin He,^{2,a)} and Zhiyuan He^{1,a)}

AFFILIATIONS

¹School of Materials Science and Engineering, Beijing Institute of Technology, Beijing 100081, People's Republic of China

²Department of Materials Science and Engineering, University of California, Los Angeles, California 90095, USA

³Longyuan (Beijing) Wind Power Engineering Technology Co., LTD, Beijing 100034, China

⁴Torch High Technology Industry Development Center, Ministry of Science and Technology, Beijing, China

^{a)} Authors to whom correspondence should be addressed: hezuy@bit.edu.cn and ximinhe@ucla.edu

ABSTRACT

Solar energy-based renewable energy conversion and storage technologies offer a great promise of combating energy shortage and transitioning to a sustainable society. Efficient collection and transformation play decisive roles in optimizing the harvest of solar energy. Photothermal conversion has emerged as the most efficient solar energy conversion technology, particularly, photothermal coatings could convert light into heat and has triggered a surge of interest in ice removal related applications. Here, we present a comprehensive review of popular documented photothermal conversion materials and the mechanisms of photothermal conversion technologies. Additionally, we pay attention to efficient light-trapping structures for outperformed solar-driven photothermal materials. After that, we investigate the mechanisms of the deicing process. Finally, we discuss the progress of photothermal deicing systems and summarize future challenges in improving their performance. This review serves as a reasonable reference for the classification of photothermal materials and the construction of light-trapping structures, providing valuable insight into the design of photothermal materials for anti-icing applications.

Published under an exclusive license by AIP Publishing. <https://doi.org/10.1063/5.0148288>

TABLE OF CONTENTS

I. INTRODUCTION	2	B. Inhibiting ice nucleation	8
II. PHOTOTHERMAL MECHANISMS	2	C. Reducing ice adhesion	9
A. Plasmonic heating	2	VI. CHALLENGES OF PHOTOTHERMAL DEICING	
B. Electron-hole generation and relaxation	2	COATINGS	10
C. Thermal vibration of molecules	3	A. Transparent photothermal deicing coatings	10
III. PHOTOTHERMAL MATERIALS	3	B. Effective combination of photothermal and other	
A. Carbon-based materials	4	deicing strategies (photothermal+ strategy)	10
B. Two-dimensional transition metal carbides		1. Combination of photothermal and slippery	
(MXenes)	4	strategies	11
C. Organic polymer materials	4	2. Combination of photothermal and	
D. Metal-based materials	5	superhydrophobic strategies	12
IV. PHOTO-THERMAL CONVERSION PARAMETERS	6	3. Combination of photothermal and phase-	
A. Light absorption—Construction of the light-		change strategies	13
trapping structures	6	4. Combination of photothermal and	
B. Heat transfer loss	6	electrothermal strategies	15
V. MECHANISMS OF DEICING	7	5. Combination of photothermal and other	
A. Preventing water adhesion	8	strategies	15
		VII. CONCLUSIONS AND PROSPECTS	15

I. INTRODUCTION

Unexpected icing may pose a serious threat to critical infrastructures, such as power lines, wind turbines, and communication towers, as well as daily vehicles such as airplanes and cars, which can lead to catastrophic accidents.^{1–5} At present, methods such as electrothermal deicing, hot air deicing, and mechanical deicing are utilized to remove ice.⁶ However, these techniques are typically energy-intensive. Chemical-based deicing methods, such as spraying salt solutions, can lower the freezing point of water and diminish ice accumulation, while the strategies would cause environmental pollution and also accompany unavoidable corrosion of metallic equipment.⁷ As an abundant renewable energy source, solar energy offers many benefits in solving the global energy shortage issue, including its broad spectrum and wide availability.^{8,9} With the phasing-out of fossil fuels due to environmental concerns, solar energy is increasingly prevalent in our daily lives.¹⁰ Photovoltaic conversion¹¹ and photothermal conversion¹² are two main ways to utilize solar energy. In this review, we focus on photothermal conversion, which refers to absorbing sunlight and converting it into thermal energy.¹³ In general, the mechanisms of photothermal conversion can be classified into three categories: plasmonic heating,¹⁴ electron–hole generation and relaxation,¹⁵ and thermal vibration of molecules.¹⁶

The efficiency of solar energy collection primarily depends on the selection of photothermal materials and the design of light-trapping surface structures.^{17,18} Photothermal materials used for deicing require adequate optical absorption across the spectrum of sunlight (295–2500 nm).¹⁹ This review covers various photothermal materials, including carbon materials,²⁰ two-dimensional (2D) non-carbonaceous materials (e.g., MXene),²¹ polymer materials,²² and metal matrix materials.²³ The sunlight absorption rate determines the photothermal conversion,²⁴ which could be improved by the design of light-trapping structures.²⁵ The structures manipulate the direction of light propagation, resulting in increased optical reflection inside the material and reduced optical reflection on the surface.²⁶ There are three typical optical trap structures, array structures,^{27,28} porous structures,²⁹ and random particle structures.³⁰

A solar anti-icing/deicing (SADI) surface is a cost-effective means of decreasing the formation of ice/frost or directly melting ice by focusing solar energy as heat.^{31,32} There are essential prerequisites, including broadband sunlight absorption, effective solar conversion excellent ice removal performance, scalable production, low cost, and long-term stability, to achieve the widespread implementation of SADI materials. However, photothermal anti-icing has practical limitations due to restricted light absorption under zero-light or weak-light conditions. Thus, a “photothermal+” strategy that combines photothermal deicing with other deicing methods is necessary to achieve satisfactory performance. The strategy is mainly employed to compensate for the lack of sunlight during the nighttime. For instance, Fig. 1 shows the combination of photothermal anti-icing and phase change energy storage techniques that can effectively deice during the day and night.³³ The photothermal material releases heat in the presence of sunlight, while phase change energy regulates the ambient temperature in the absence of light. The combination of photothermal and electrothermal anti-icing strategies can also provide uninterrupted ice-free performance throughout the day by electrothermally providing heat during nighttime.³⁴ The two techniques complement each other. In addition, the combination of the photothermal and

superhydrophobic strategies can quickly remove ice from the surface.³⁵ This is achieved by melting the accumulated ice through the photothermal effect and allowing the melted water to slide off from the superhydrophobic surface (SHS) layer. This approach reduces the adhesion strength of ice on the photothermal material surface and offers a promising prospect for anti-icing applications in extreme environments.³⁶

In this review, recent works on photothermal deicing coating strategies are spotlighted. Here, we begin with a discussion of multiple photothermal mechanisms. After that, photothermal materials with different photothermal conversion mechanisms are overviewed and classified. In the third part, we introduce three types of light-trapping structures that have been witnessed to improve sunlight absorption. Fourth, different deicing mechanisms are investigated. Fifth, the research progress of photothermal deicing coatings is presented. Finally, we conclude the review by outlining potential challenges and future research directions of photothermal coatings for anti-icing/deicing applications. We hope this review can facilitate the understanding and development of photothermal deicing.

II. PHOTOTHERMAL MECHANISMS

The process of photothermal conversion is a complicated and interconnected series of stages. It involves several steps, including the absorption of light, conversion of photon energy to heat energy through phonons, transferring heat through bulk phase and interface of materials, and causing phase transformations in substances. When photons interact with electrons in the material, the electrons absorb photon energy through energy level transition or plasmon resonance, resulting in high-energy electrons in the excited state, also known as hot electrons.^{37–39} These hot electrons tend to return to a state of thermal equilibrium by transferring and redistributing some of their energy through secondary radiation or vibrational relaxation. This transition of electrons to excited states and the restoration of thermal equilibrium result in the production and diffusion of heat energy, often leading to an increase in temperature.³⁸ In general, the mechanisms of photothermal conversion can be classified into three categories: plasmonic heating,¹⁴ electron–hole generations and relaxation,¹⁵ and thermal vibration of molecules.¹⁶

A. Plasmonic heating

Compared to other materials, metals typically have a high concentration of free electrons. When a metal's surface is exposed to a photon of a particular wavelength, the electrons can collectively oscillate in response to the photon's electric field, which leads to a phenomenon known as the local surface plasmon resonance effect (LSPR). This effect enhances the scattering and absorption of incoming photons [as shown in Fig. 2(a₁)],³⁹ resulting in the release of heat through a process called the plasma photothermal effect. Within a short period (1–100 fs), the generated hot carriers undergo electron–electron relaxation, electron–phonon relaxation, and phonon–phonon relaxation,⁴⁰ ultimately converting light energy into heat energy [as depicted in Fig. 2(a₂)].

B. Electron–hole generation and relaxation

As solar photons come to interact with semiconductors that have a narrow bandgap, the electrons in the valence band (VB) get stimulated to move up to the conduction band (CB) since the solar energy

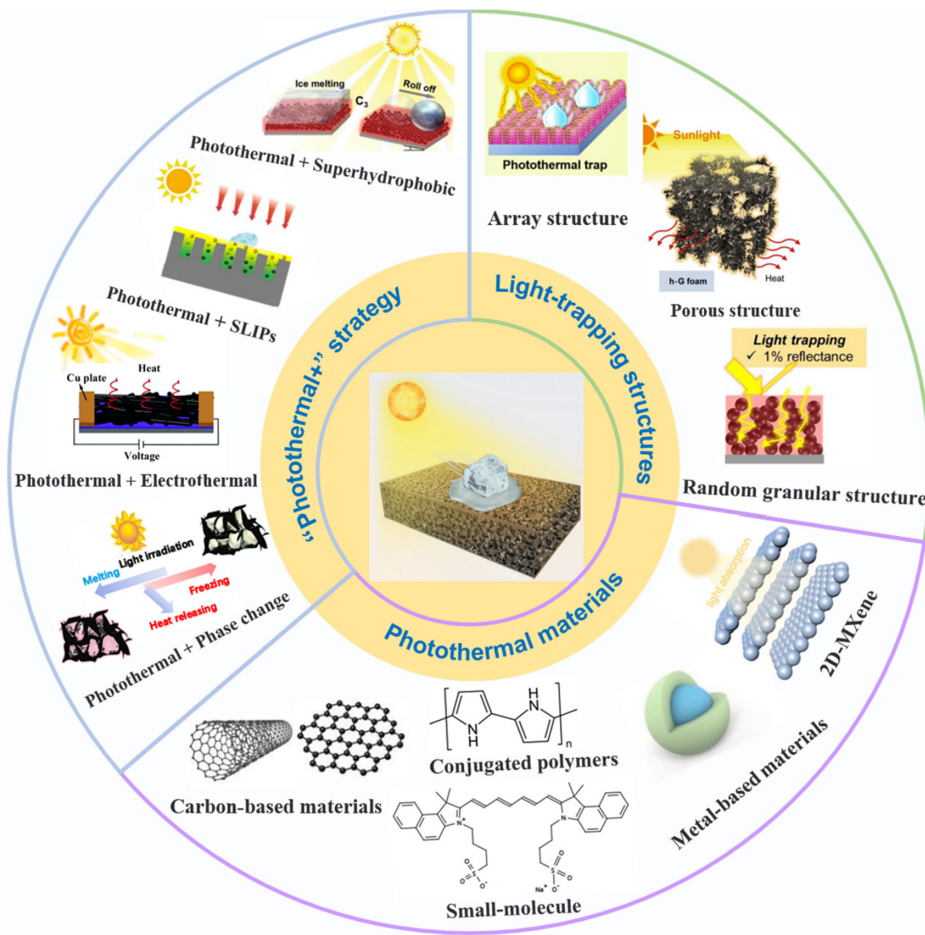


FIG. 1. Schematic diagram of the scope of the review.

surpassed the bandgap of the materials, producing excited electrons and holes in the CB and VB, respectively. The excess energy is then transformed into heat via non-radiative mechanisms as the excited electrons and holes relax to the corresponding CB and VB edges [Fig. 2(b₁)].^{39,41} However, for direct bandgap materials, the radiative recombination of electrons and holes leads to the loss of photothermal performance through the release of photons. Generally, the optical absorption of a semiconductor can be enhanced by introducing in-band energy states, reducing the bandgap, and creating LSPR through heteroatom doping, as shown in Fig. 2(b₂).⁴²

C. Thermal vibration of molecules

Materials with abundant conjugated π bonds can absorb photon energy, causing their electrons to become excited and then move from the ground state π orbital to the higher excited π^* orbital, as shown in Fig. 2(c₁).³⁹ The heat is released when the excited electron relaxes back to its ground state. By incorporating additional components into the conjugated polymer, as depicted in Fig. 2(c₂), not only the range of light absorption can be broadened, but the photoluminescence (PL) emission of the conjugated polymer can also be inhibited. As a result, the photothermal conversion efficiency of the resulting photothermal composite is improved.⁴³

The photothermal conversion efficiency (η) is an important parameter for the evaluation of the performance of photothermal material, which refers to the material's ability to absorb external radiation and produce phonons. The efficiency (η) can be determined using the following formula:

$$\eta = \frac{hS(T_{max} - T_{surr}) - Q_{dis}}{I(1 - 10^{-a})}, \quad (1)$$

where T_{max} and T_{surr} represent the highest temperature of the solute and ambient temperature, respectively. The thermal conductivity, the area of the sample, and heat dissipation caused by the absorption of light by the sample are denoted as h , S , and Q_{dis} , respectively. I refers to the intensity of the incident light, λ is the wavelength, and a is the absorbance of the sample.

III. PHOTOTHERMAL MATERIALS

In general, a good material candidate for photothermal conversion should absorb sunlight with negligible transmittance and reflectance across the full solar spectrum range (295–2500 nm) while converting the solar energy to heat energy efficiently without undergoing any energy transformation or reradiation. Ultra-black or super-black materials induced by small conductors are surfaces that can

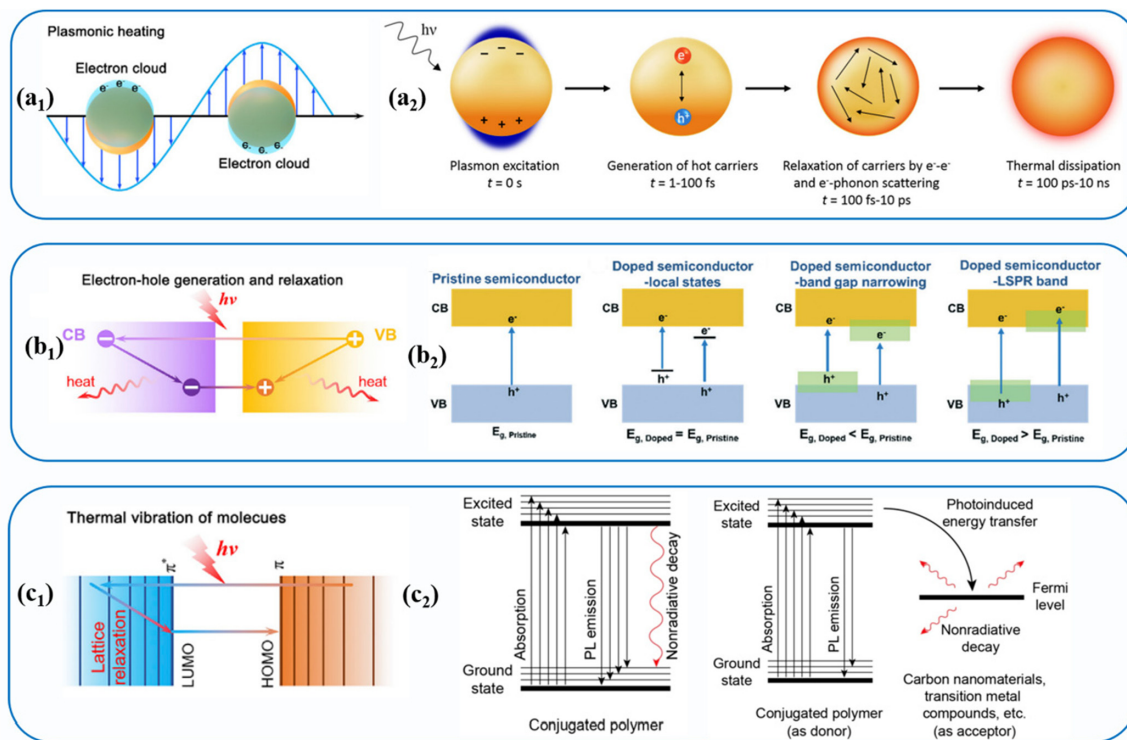


FIG. 2. Photothermal mechanisms: (a₁) plasmonic heating;³⁹ (a₂) dynamics of plasmon decay and time evolution of charge carriers;⁴⁰ (b₁) electron-hole generation and relaxation;³⁹ (b₂) band structure of doped semiconductors;⁴² (c₁) thermal vibration of molecules;⁴³ (c₂) photothermal generation from an original conjugated polymer and conjugated polymer matrix composites.⁴³ Panel (a₁) reproduced with permission from Chen *et al.*, *Joule* **3**, 683–718 (2019). Copyright 2019 Elsevier Ltd. Panel (a₂) reproduced with permission from Ahlawat *et al.*, *Commun. Mater.* **2**, 114 (2021). Copyright 2021 Author(s), licensed under a Creative Commons Attribution. Panel (b₁) reproduced with permission from Chen *et al.*, *Joule* **3**, 683–718 (2019). Copyright 2019 Elsevier Ltd. Panel (b₂) reproduced with permission from Liu *et al.*, *Environ. Sci.: Nano* **9**, 2264–2296 (2022). Copyright 2022 Royal Society of Chemistry. Panel (c₁) reproduced with permission from Chen *et al.*, *Joule* **3**, 683–718 (2019). Copyright 2019 Elsevier Ltd. Panel (c₂) reproduced with permission from Xiao *et al.*, *ACS Appl. Polym. Mater.* **2**, 4273–4288 (2020). Copyright 2020 American Chemical Society.

absorb nearly all incoming light, including visible and infrared light, resulting in an extremely dark or black appearance.⁴⁴ These materials are fabricated by constructing a surface composed of densely packed, subwavelength-sized conductive structures, commonly made from metals or carbon nanotubes (CNTs), which are designed to trap and absorb incident light across all angles and wavelengths.^{45,46} We categorize ultra-black materials into four distinct groups: carbon-based materials, two-dimensional transition metal carbides (MXenes), organic polymer materials, and metal-based materials.

A. Carbon-based materials

Carbon-based materials can absorb sunlight in the full solar spectral range (295–2500 nm) with a high solar absorption rate, excellent structural tunability, and processability, showing competitive advantages in the field of photothermal conversion. These properties are mainly attributed to their conjugated structures, which allow for strong absorption of infrared radiation. When these materials absorb light energy, the π electrons in their bonding molecular orbital transition to the π^* orbital. As the excited electrons decay to the ground state, they release part of the absorbed energy in the form of heat, resulting in the photothermal effect.⁴² Commonly used artificial carbon materials include the graphene family [graphite, graphene, carbon

nanotubes (CNTs)], and carbon-based composites.⁴⁷ To enhance sunlight collection, various nanostructures in which the incident light can be trapped have been developed, such as vertically aligned, porous, and layered nanostructures [Fig. 3(a)].

B. Two-dimensional transition metal carbides (MXenes)

Recently, 2D materials MXenes have demonstrated a unique and appealing photothermal conversion performance, as shown in Fig. 3(b).⁴⁸ Specifically, the photothermal conversion efficiency of $\text{Ti}_3\text{C}_2\text{T}_x$ is estimated to be about 100%.⁴⁹ Such a high conversion efficiency is benefited tremendously from its electromagnetic interference shielding effect⁵⁰ and LSPR effect,⁵¹ which can effectively absorb solar energy and convert it into heat energy for storage and utilization. To tackle the intrinsically high conversion efficiency, studies of photothermal MXenes are still in their infancy, and further investigation is required to unravel the mechanism responsible for its high conversion efficiency.⁵²

C. Organic polymer materials

At present, the organic photothermal materials mainly include conjugated polymers (polypyrrole, polydopamine, polyaniline, etc.)

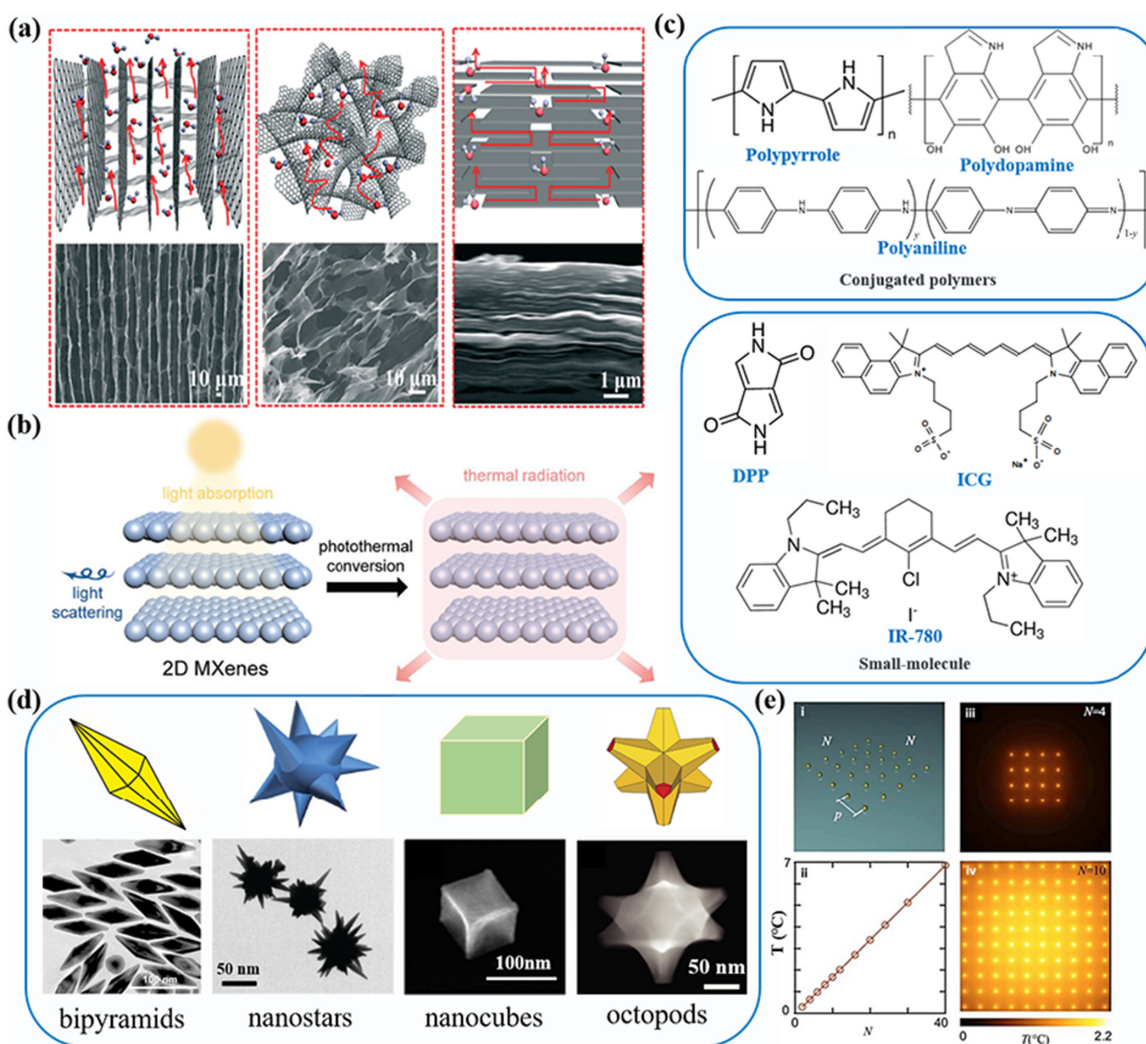


FIG. 3. (a) Improvement of light absorption by using arrayed, porous, hierarchical carbon-based nanostructures;²⁸ (b) schematic illustration of photothermal conversion in 2D MXenes;⁵² (c) molecular structure of two typical organic polymer materials, including conjugated polymers (top) and small molecule (bottom); (d) graphical structures and relevant SEM (scanning electron microscopy) images of gold nanoparticles with different shapes such as bipyramids,⁵⁴ nanostars,^{55,56} nanocubes,⁵⁷ and octopods;⁵⁸ and (e) improvement of photothermal conversion efficiency by plasma coupling.⁵⁹ Panel (a) reproduced with permission from Zhang *et al.*, *ACS Nano* **11**, 5087–5093 (2017). Copyright 2017 American Chemical Society. Panel (b) reproduced with permission from Xu *et al.*, *Adv. Funct. Mater.* **30**, 2000712 (2020). Copyright 2020 Wiley-VCH. Panel (d) reproduced with permission from Lou-Franco *et al.*, *Nano-Micro Lett.* **13**, 10 (2020). Copyright 2020 Springer Nature. Panel (d) reproduced with permission from Kim *et al.*, *Nanoscale* **8**, 987–994 (2016). Copyright 2016 Royal Society of Chemistry and Cheng *et al.*, *Mater. Chem.* **22**, 2244–2253 (2012). Copyright 2012 Royal Society of Chemistry. Panel (d) reproduced with permission from Rycenga *et al.*, *Nano Lett.* **12**, 6218–6222 (2012). Copyright 2012 American Chemical Society. Panel (d) reproduced with permission from Ringe *et al.*, *Sci. Rep.* **5**, 17431 (2015). Copyright 2015 Springer Nature. Panel (e) reproduced with permission from Baffou *et al.*, *Phys. Rev. B* **82**, 165424 (2010). Copyright 2010 American Physical Society.

and small molecular dyes such as diketopyrrolopyrrole (DPP), indocyanine green (ICG), and IR780, as shown in Fig. 3(c). Most polymeric photothermal conversion materials have conjugated chemical structures. When photoexcited, the excited electrons can migrate freely along the conjugated π skeleton in the polymer backbone and can be captured by energy receptors at any site, resulting in efficient energy transfer. Polymeric photothermal conversion materials are characterized by excellent photothermal performance, diverse structures, and

ease of surface modification, all of which make them potential candidates for practical applications.¹⁹

D. Metal-based materials

Metal-based photothermal materials mainly include metal nano-materials (Au, Ag, Pt, Pd, etc.) and their compounds (Fe_3O_4 , CuS, TiN, etc.).⁵³ Metallic materials have a unique LSPR effect. When

precious metal nanoparticles (NPs) are exposed to light with a frequency that matches the overall vibration frequency of the metal's electrons, they absorb the photons and generate heat. However, the plasma resonance effects of precious metal particles are limited to a specific wavelength range, restricting their utility in solar energy conversion.⁴² To improve the photothermal conversion efficiency of LSPR-based materials, various approaches can be employed. For instance, modifying the shape of the metal nanoparticles can adjust the absorption bandwidth, as illustrated in Fig. 3(d). Additionally, generating plasma coupling by using resonance modes of metal NPs, as depicted in Fig. 3(e), can lead to remarkable photothermal effects in the gap between two metal nanoparticles positioned in proximity to each other with spacings smaller than their diameter.

IV. PHOTOTHERMAL CONVERSION PARAMETERS

A. Light absorption—Construction of the light-trapping structures

Light absorption has an important effect on photothermal conversion. In addition to the inherent absorption properties of the materials, design and preparation of a light-trapping structure, which changes the light propagation direction, can achieve frustrated total internal reflection and thus effectively improve light absorption.⁶⁰ The incident light would be trapped inside the structure, and the energy loss of internally reflected light can be reduced by extending the optical path length.^{61,62} Moreover, the light-trapping structures lead to a reduction in transmittance,²⁹ ultimately maximizing light absorption by fully reducing surface reflection and transmission.⁶³ Common light-trapping structures include array structures, porous structures, and random particle structures.

The array structure is among the most studied light-trapping structure for boosting sunlight absorption. Xie *et al.* fabricated a ST@CA/CC surface that utilizes an array structure to increase sunlight absorption, resulting in a ~99% absorption rate across the entire solar spectrum. The surface features a dense and uniformly distributed array of carbon nanowires on a carbon fiber substrate, which enhances light absorption through the light-trapping effect, as shown in Fig. 4(a₁).⁶⁴ Figure 4(a₂) shows a multifunctional magneto-responsive photothermal composite cilia array (MRPA) that also utilizes a light-trapping array to remove ice accretion.⁶⁵ The photothermal multiwalled carbon nanotubes (CNTs) coating layer in the MRPA contains micro/nanoscale hierarchical structures and magnetic composites, allowing it to generate enough heat by converting absorbed sunlight.

The porous structure offers an enhanced light absorption ability through the effects of light trapping and multiple scattering events, as shown in Fig. 4(b₁). There are two common ways to construct porous structures. The ice template method represents an important one due to its widespread availability, environmental friendliness, and simple control process of the pore structure. Using oriented ice crystals as templates, one can design the pore structure of porous materials by controlling the nucleation and growth of ice crystals.⁶⁶ The process is illustrated in Fig. 4(b₂), where precursor monomers/polymers are squeezed together as ice crystals grow from the bottom up in the presence of a surrounding temperature gradient, leading to dense polymeric pore walls at the grain boundaries of the growing ice crystals. Porous channels with distinct orientations have also been observed in Photothermal Macroporous Xerogels (PMX) due to the oriented growth of ice crystals along the temperature gradients.⁶⁷ In addition,

commercial white sugar particles could also be employed as pore templates.⁶⁸ Figure 4(b₃) shows a porous paraffin/polydimethylsiloxane (PDMS)/reduced graphene oxide (rGO) material prepared with a sugar template. The PDMS/rGO coating is capable of using solar illumination for *in situ* deicing. The size of the pores can be tailored by selecting sugar particles with different sizes.

In terms of the random particle structure, the particles can be the same or of different sizes. Zhang *et al.* prepared virus-like graded micro-nano structures that are uniform in size. The particles in this structure resemble virus on a micrometer scale, with a diameter of approximately 1 μm and nanoscale protrusions measuring 30 nm in diameter.⁶⁹ These particles are loosely stacked on the top of each other, leaving microscale voids left on the surface [Fig. 4(c₁)].⁶⁹ The virus-like nanoparticles can significantly reduce outward reflections and harvest near-infrared radiation through multiple internal reflections between the nanoscale protrusion and microscale particles. Another example of a random granular structure is shown in Fig. 4(c₂), which is composed of interconnected soot particles with a typical diameter of 100 nm.⁷⁰ The candle soot particles provide hierarchical nano/microstructures, which release heat via the photothermal effect to melt accumulated ice when illuminated by sunlight, as shown in Fig. 4(c₂).

B. Heat transfer loss

In addition to enhancing light absorption, it is also important to reduce the heat transfer losses. The primary sources of energy loss during the photothermal conversion process are thermal conduction, convection, and radiation loss.⁷²

Heat conduction is the process where heat is transferred from hotter to colder regions within an object due to molecular collisions.⁷³ The following formula describes the heat transferred per unit time during the heat conduction process through solid materials and can be utilized to calculate the heat conduction loss for materials or structures at a specific temperature difference:

$$Q = kA \frac{T_1 - T_2}{d}, \quad (2)$$

where k stands for heat conduction coefficient; A represents heat transfer area; T_1 and T_2 represent the temperature on both sides, respectively; and d is the heat transfer distance.

To mitigate heat conduction losses, possible solutions include: utilizing materials with low thermal conductivity; increasing the material's thickness; and decreasing the heat conduction area.⁷⁴

Heat convection involves the transfer of heat via fluid motion.⁷⁵ During the photothermal conversion process, heat convection typically results from energy loss due to convective circulation created by the rising of hot air and the sinking of cold air. The subsequent formula can be used to calculate the heat convection loss:

$$Q = hA(T_s - T_{inf}), \quad (3)$$

where Q is heat convection loss; h is convective heat transfer coefficient; A is the heated surface area; T_s is the surface temperature; and T_{inf} is the ambient temperature.

To decrease heat convection loss, certain steps can be implemented, including constructing insulation around the system and regulating the air flow speed.^{76,77}

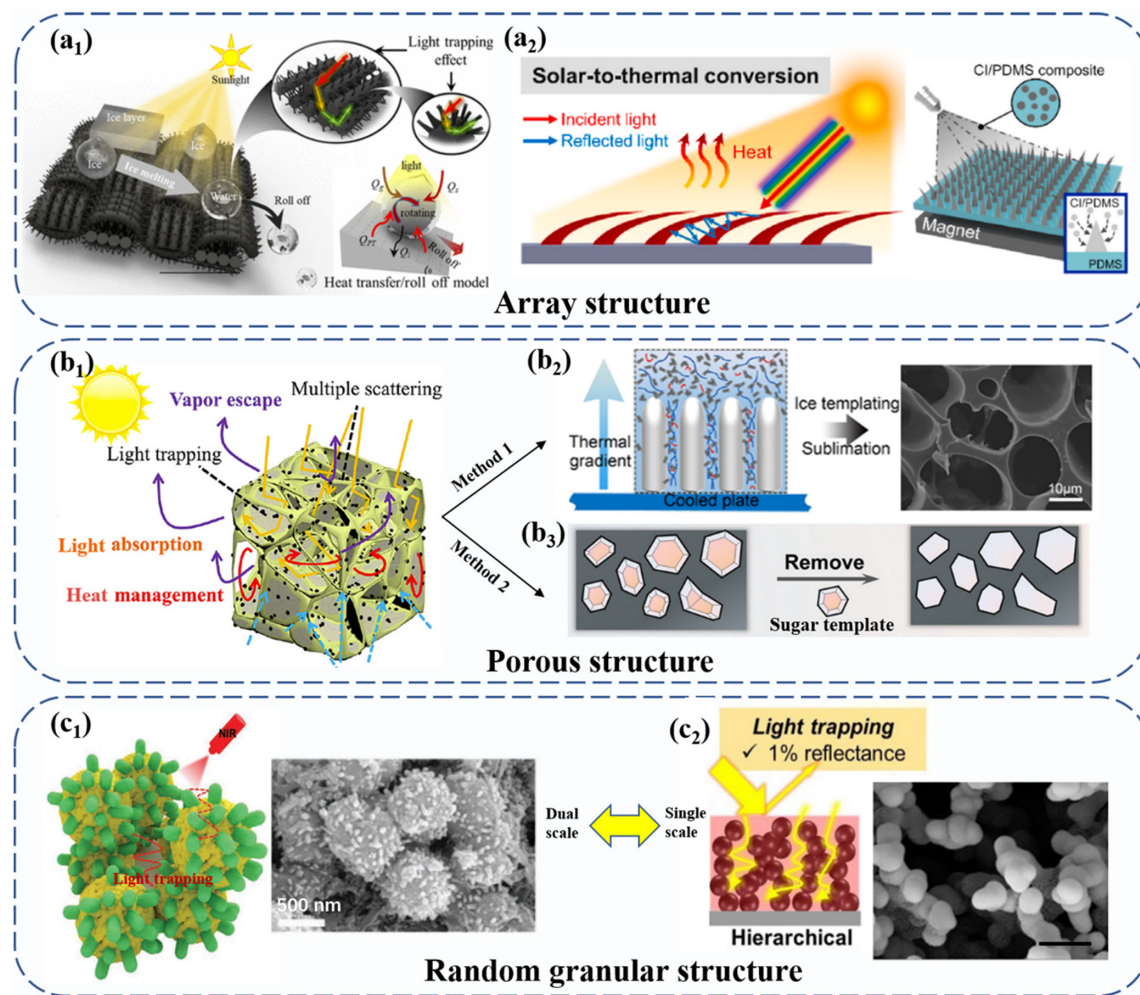


FIG. 4. Three kinds of photothermal trap structures for enhanced optical absorption: array structure, porous structure, and random particle structure. The array structure is formed by (a₁) electrochemical deposition of carbon nanowires⁶⁴ and (a₂) spontaneously arranging the magnetic particle solution along the direction of the magnetic field.⁶⁵ The (b₁) light-trapping porous structure⁷¹ can be constructed by (b₂) the ice template method of vertical directional freezing⁶⁷ and (b₃) removing the physical pore-forming agent method of sugar particles.⁶⁸ The random granular structure is formed by (c₁) two different size particles⁶⁹ and (c₂) single size particles.⁷⁰ Panel (a₁) reproduced with permission from Xie *et al.*, *ACS Appl. Mater. Interfaces* **13**, 48308–48321 (2021). Copyright 2021 American Chemical Society. Panel (a₂) reproduced with permission from Lee *et al.*, *Compos. Sci. Technol.* **217**, 109086 (2022). Copyright 2021 Elsevier Ltd. Panel (b₁) reproduced with permission from Gu *et al.*, *Nano Energy* **74**, 104857 (2020). Copyright 2020 Elsevier Ltd. Panel (b₂) reproduced with permission from Yu *et al.*, *ACS Appl. Mater. Interfaces* **13**, 37609–37616 (2021). Copyright 2021 American Chemical Society. Panel (c₁) reproduced with permission from Zhang *et al.*, *Adv. Funct. Mater.* **32**, 2201795 (2022). Copyright 2022 Wiley-VCH.

Thermal radiation is the process of heat transfer via electromagnetic waves, which does not necessitate a medium. When an object's temperature is above absolute zero, it emits heat energy into its surroundings.⁷⁵ As per the Stefan–Boltzmann law illustrated in formula (4), the energy of thermal radiation is proportional to the temperature's fourth power, implying that an object with a higher temperature releases more energy,

$$j^* = \epsilon \sigma T^4. \quad (4)$$

The proportionality coefficient σ is called the Stefan constant; ϵ is the radiation coefficient of black body; if absolute bold, $\epsilon = 1$;

T stands for absolute temperature. To minimize thermal radiation loss, certain strategies can be employed to enhance photothermal conversion efficiency. For instance, choosing materials with lower absorptivity and higher reflectivity can reduce the amount of light energy absorbed.⁷⁸ By employing these methods in combination, the energy conversion efficiency of the photothermal conversion system can be enhanced.

V. MECHANISMS OF DEICING

So far, based on different stages of icing, three main approaches have been reported to achieve anti-icing on material surfaces: (1) prior

to icing, preventing the surface from coming into contact with water droplets by directly eliminating water from the surface, (2) during icing, slowing down the nucleation of ice in water droplets to extend the icing time, and (3) after icing, minimizing the adhesion between the formed ice and the surface of the material.

A. Preventing water adhesion

There are three different methods for removing water droplets from surfaces: direct rolling, self-jumping, and rolling off a liquid lubricating layer. Each method has its unique mechanism and application. Direct rolling is most effective for water droplets at the macro scale or flowing water. Due to the low contact angle hysteresis ($CAH < 5^\circ$) of the surface, moving water droplets are forced to rebound or roll-off the surface prior to freezing. Self-jumping refers to the self-migration of tiny water droplets formed by micro-water vapor condensation in the condensing environment.⁷⁹ Surfaces with superhydrophobic properties can cause these droplets to merge and release surface energy, which allows them to self-migrate and jump off the

surface. Alternatively, water droplets can also jump off the surface due to the small critical rolling radius on the superlubricated surface.

B. Inhibiting ice nucleation

For water to transition into a more thermodynamically stable state by freezing, ice nuclei must initially form in the water that possesses a molecular structure similar to that of ice. However, the growth of these ice nuclei leads to an increase in interfacial energy between the ice and water, thereby reducing the thermodynamic favorability of further growth. This rise in interfacial energy opposes the natural tendency of water to freeze, creating a specific energy barrier for ice nucleation.⁸⁰ Once an ice nucleus grows to a critical size, the favorability of ice growth surpasses the increase in interfacial energy, and the energy barrier is eliminated, leading to complete freezing.⁸¹ Nucleation can be generally divided into homogeneous nucleation and heterogeneous nucleation [Fig. 5(a)].⁸² Homogeneous nucleation occurs spontaneously through the random arrangement of molecules, while heterogeneous nucleation involves the formation of critical ice

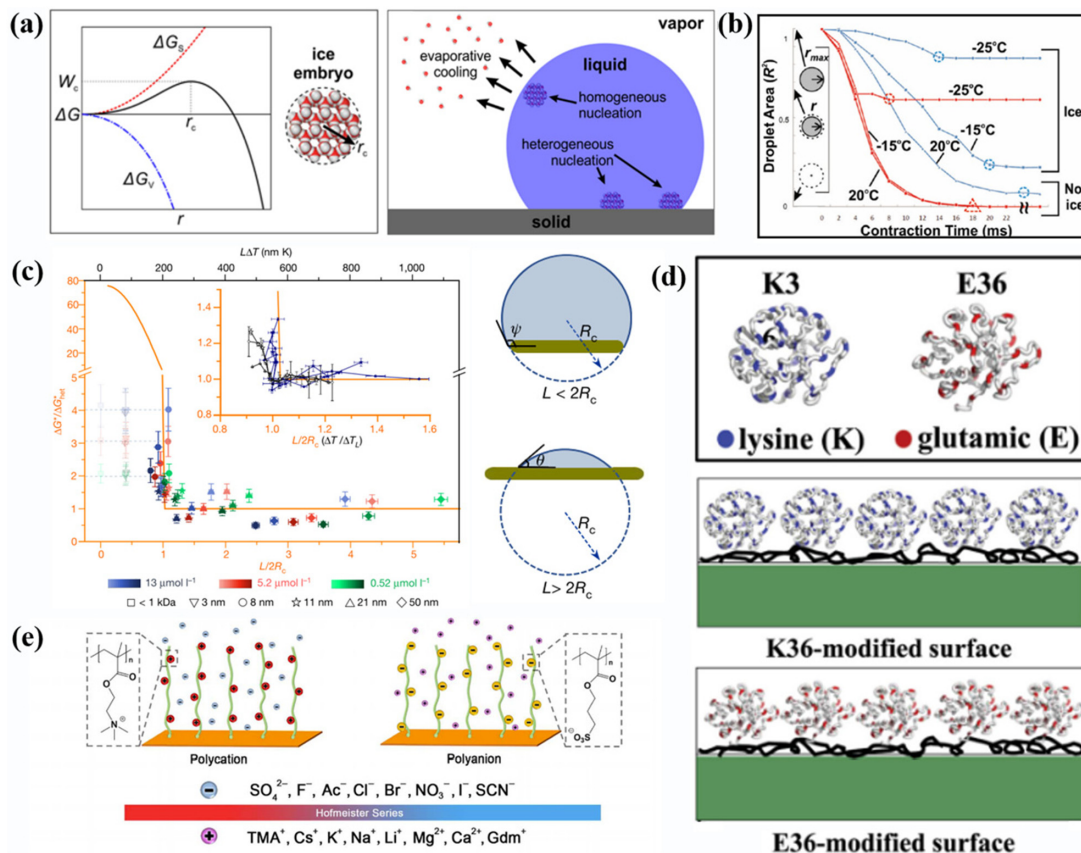


FIG. 5. Interface control ice nucleation: (a) ice nucleation can be formed through both homogeneous and heterogeneous nucleation;⁸² (b) the relation between the contact area and the contact time of a droplet hitting a supercooled surface;⁸³ (c) graphene oxide with a size smaller than the critical ice core can inhibit the nucleation of graphene oxide;⁸⁷ (d) study on the effect of charge on ice nucleation by grafting stretched supercharged unfolded polypeptides onto a solid surface;⁵⁶ and (e) polyelectrolyte brush with different resistance to anion and cation for regulating ice nucleation.⁹⁰ Panel (a) reproduced with permission from Schutzius *et al.*, *Langmuir* **31**, 4807–4821 (2015). Copyright 2015 American Chemical Society. Panel (b) reproduced with permission from Mishchenko *et al.*, *ACS Nano* **4**, 7699–7707 (2010). Copyright 2010 American Chemical Society. Panel (c) reproduced with permission from Bai *et al.*, *Nature* **576**, 437–441 (2019). Copyright 2019 Nature. Panel (d) reproduced with permission from Yang *et al.*, *Adv. Mater.* **28**, 5008–5012 (2016). Copyright 2016 Wiley-VCH.

nuclei on external surfaces. Homogeneous nucleation has a higher nucleation barrier than heterogeneous nucleation when there is no external interference.

Heterogeneous nucleation can be described by classical nucleation theory, and the nucleation rate can be expressed by the following formula:

$$J(T) = K(T)A \exp\left(\frac{-\Delta G(T)}{k_B T}\right), \quad (5)$$

where $K(T)$ is the dynamic preschool factor, A represents the contact area between the droplet and the substrate, $\Delta G(T)$ represents the Gibbs free energy barrier, k_B represents the Boltzmann constant, and T represents the substrate temperature.

According to classical nucleation theory, it is possible to prevent heterogeneous nucleation by reducing the contact area between a droplet and a substrate and increasing the nucleation energy barrier. As shown in Fig. 5(b), when supercooled water drops are disturbed by external stimuli, they quickly freeze and adhere to most surfaces,⁸³ making it important to minimize their contact time with surfaces to prevent ice nucleation.^{84,85} By altering the material's surface roughness, ice–water interfacial tension, and volume Gibbs free energy difference, the heterogeneous nucleation energy barrier can be raised.⁸⁶ Bai *et al.* used graphene oxide as a substrate to control ice nuclei behavior⁸⁷ and found that a size around 11 nm was effective in promoting heterogeneous nucleation [Fig. 5(c)]. As shown in Fig. 5(d), Yang *et al.* grafted supercharged unfolded polypeptides on solid surfaces to study their charge effect on ice nucleation and found that

positively charged polypeptides stimulated ice nucleation, while negatively charged polypeptides prevented it.⁸⁸ According to the classical nucleation theory, supercharged polypeptides can not only change the electrostatic energy density between ice nuclei and water of the same volume through the action of an electric field but also change the surface tension between ice nuclei and water through the substrate.⁸⁹ Therefore, the presence of overcharged peptides can change the nucleation barrier of ice. A significant issue in realistic applications is the impact of ions on the heterogeneous nucleation and ice formation of supercooled water. He *et al.* discovered the Hofmeister effect, which involves adjusting counterions on polyelectrolyte surfaces to control nucleation and ice formation of supercooled water by affecting the dynamic behavior and static structure of interfacial water during the production of ice and supercooled water [Fig. 5(e)].⁹⁰

C. Reducing ice adhesion

Figure 6(a) depicts two types of ice adhesion, namely, intrinsic adhesion and macroscopic adhesion.⁹¹ Icephobic coatings have been developed to reduce the adhesion between the ice sheet and the surface. Strategies for lowering the ice surface adhesion strength include employing smooth, textured, slippery, and interfacial crack source surfaces.⁹²

- (1) Smooth surfaces usually refer to uniform surfaces composed of polymers with a low elastic modulus and low surface energy. When an interface between ice and a substrate slides, dynamic stick-slip movement of the ice under the action of tangential

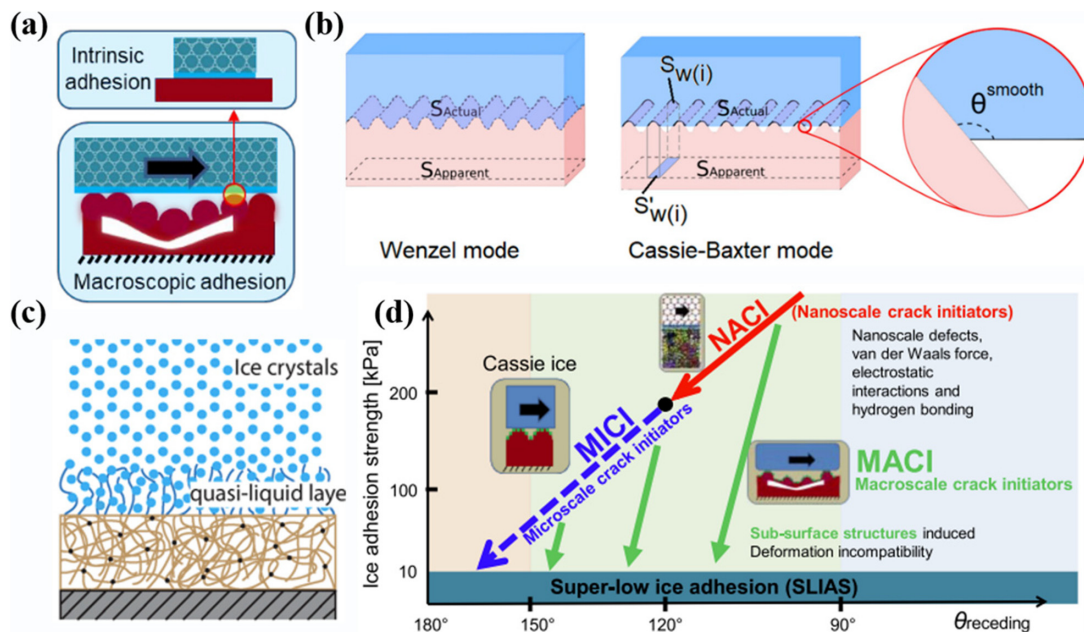


FIG. 6. Ice adhesion mechanics: (a) intrinsic ice adhesion and macroscopic ice adhesion;⁹¹ (b) schematic diagram of rough substrate wetting in different modes;⁹⁴ (c) a quasi-liquid layer that forms at the interface serves as a lubricant to create effective low-ice adhesion;⁹⁵ (d) macro crack initiator (MACI) design for extremely low ice adhesion.⁹¹ Panel (a) reproduced with permission from Zhuo *et al.*, *Chem. Eng. J.* **405**, 127088 (2021). Copyright 2021 Elsevier Ltd. Panel (b) reproduced with permission from Emelyanenko *et al.*, *Coatings* **10**, 648 (2020). Copyright 2020 Author(s), licensed under a Creative Commons Attribution. Panel (c) reproduced with permission from Chen *et al.*, *ACS Appl. Mater. Interfaces* **9**, 4202–4214 (2017). Copyright 2017 American Chemical Society. Panel (d) reproduced with permission from Zhuo *et al.*, *Chem. Eng. J.* **405**, 127088 (2021). Copyright 2021 Elsevier Ltd.

force leads to debonding, thus forming an air cavity at the interface. The propagation of this air cavity leads to further stick-slip movement, reducing ice adhesion strength.⁹³ The formula used to estimate ice adhesion strength on these surfaces is as follows:

$$\tau_{ice} \propto \sqrt{\frac{W_{adh}\mu}{t}}, \quad (6)$$

where W_{adh} is the adhesive strength work between ice and material, μ is the shear modulus of the material, and t is the thickness of the film. The formula indicates that materials with low surface energy and low shear modulus can be used to create surfaces with low ice adhesion strength.

- (2) Layered structures, such as superhydrophobic surfaces (SHS) and hydrophobic surfaces, are typically present in textured surfaces with ice repellency. In the case of hydrophobic surfaces, the molecular interaction leads to significantly low ice adhesion. The adhesion work (W_a) of liquid and solid in contact correlates with the contact angle, as shown in the formula:

$$W_a = \gamma_{lv}(1 + \cos \theta_e), \quad (7)$$

where γ_{lv} is the liquid-vapor surface tension, and θ_e is the equilibrium contact angle. W_a of liquid water is often directly related to the ice adhesion strength to the surface. The premise of SHS with reduced ice adhesion is the presence of a Cassie wetting state, as shown in Fig. 6(b).⁹⁴

- (3) The effectiveness of reducing ice adhesion through lubrication primarily relies on the material's capacity to accommodate ice with a smooth interface. The existence of a liquid layer can serve as a lubricant when ice forms on such a smooth surface, reducing the contact between the ice and the underlying substrate [Fig. 6(c)].⁹⁵ The resist icing ability of the device/system can be impacted by both the substrate and the interfacial lubricating layer.
- (4) According to the classical fracture mechanics theory, ice adhesion strength can be expressed as

$$\tau = \sqrt{EG/(\pi a\Lambda)}, \quad (8)$$

where G is the surface energy, E is the apparent Young's modulus, a is the total crack length, and Λ is a dimensionless constant.

Generating cracks at the interface between ice and substrate shows promise as an effective method for achieving low ice adhesion. Based on the principle of fracture mechanics, a surface containing crack initiators was prepared at the ice-substrate interface, which enhanced the generation of cracks and effectively reduced the adhesion of ice [Fig. 6(d)].^{91,96}

VI. CHALLENGES OF PHOTOTHERMAL DEICING COATINGS

Ice accumulating on exposed surfaces is common in cold weather and compromises the normal operations of devices and facilities. To overcome this issue, photothermal anti-icing surfaces are a preferred solution due to their cost-effectiveness, excellent energy-saving benefits, and eco-friendliness. However, it is still challenging to improve

the conversion efficiency of photothermal coatings, overcome the limitation of solar radiation intermittence, and achieve high visible light transmittance in photothermal systems.

A. Transparent photothermal deicing coatings

One critical issue that plagued the development of photothermal anti-icing/deicing surfaces for long-time employment is poor transparency. Photothermal deicing coatings should be opaque and/or black since transparent objects barely absorb light.^{97,98} However, it is highly desirable to have good transparency for deicing/defrosting surfaces used in telescope lenses, windows, windshields, electronic displays, and solar cells.^{99,100} Over the past five years, some inspiring works have reported transparent photothermal coatings, which are summarized in Fig. 4.

Au nanoparticles embedded in TiO₂ were used to create metasurfaces that strike a balance between optical transparency and light absorption. By employing a subwavelength-thick LSPR material with broadband visible light absorption, the metasurfaces are able to maintain some level of transparency even under freezing conditions. One study found that concentrating solar energy on the surface causes a notable increase in temperature, exceeding 10 °C, enabling rapid deicing within 30 s.¹⁰¹ Similarly, Walker *et al.* also designed a metasurface using Au nanoparticles and TiO₂ which exhibits outstanding defogging and antifogging properties through a comparable process.¹⁰²

The technique of layer-by-layer (LBL) assembly offers a new possibility for forming coatings that balance the photothermal effect and transparency. It involves stacking alternating layers of two materials that possess opposite charges through electrostatic attraction.¹⁰³ This allows for easy adjustment of the coating's thickness and structure, which provides a convenient method to balance both the photothermal effect and light transmittance. Researchers have used this technique to create transparent photothermal icephobic surfaces by assembling poly (acrylic acid) with a negative charge and polypyrrole nanoparticles with a positive charge.¹⁰⁴ In addition, the multilayer structure consisting of negatively charged Ti₃C₂T_x MXene and positively charged poly(diallyldimethylammonium) also shows excellent photothermal properties and transparency.¹⁰⁵

The majority of the existing photothermal materials utilize a broad spectrum of solar energy. Unfortunately, ideal transparent photothermal coatings require a high degree of spectral selectivity, specifically high infrared band absorption (0.75–2.5 μm) and high visible band transmittance (0.38–0.75 μm). By incorporating cesium-doped tungsten trioxide and benzotriazole NPs into thin resin films, Li *et al.* constructed a highly transparent photothermal coating. The coating provides up to 82% visible light transmittance and high UV and near-infrared light absorption (90%), resulting in significant photothermal and defogging capabilities.¹⁰⁶ Recently, Dimos *et al.* synthesized a transparent photothermal coating that selectively absorbs light to inhibit fogging, which refers to placing a gold nanofilm between two dielectric TiO₂ nanolayers (Fig. 7).¹⁰⁷

B. Effective combination of photothermal and other deicing strategies (photothermal+ strategy)

Although photothermal deicing offers obvious benefits, there are drawbacks to consider. One significant issue is that the melted water stays on the surface and can refreeze when the lighting is not constant.

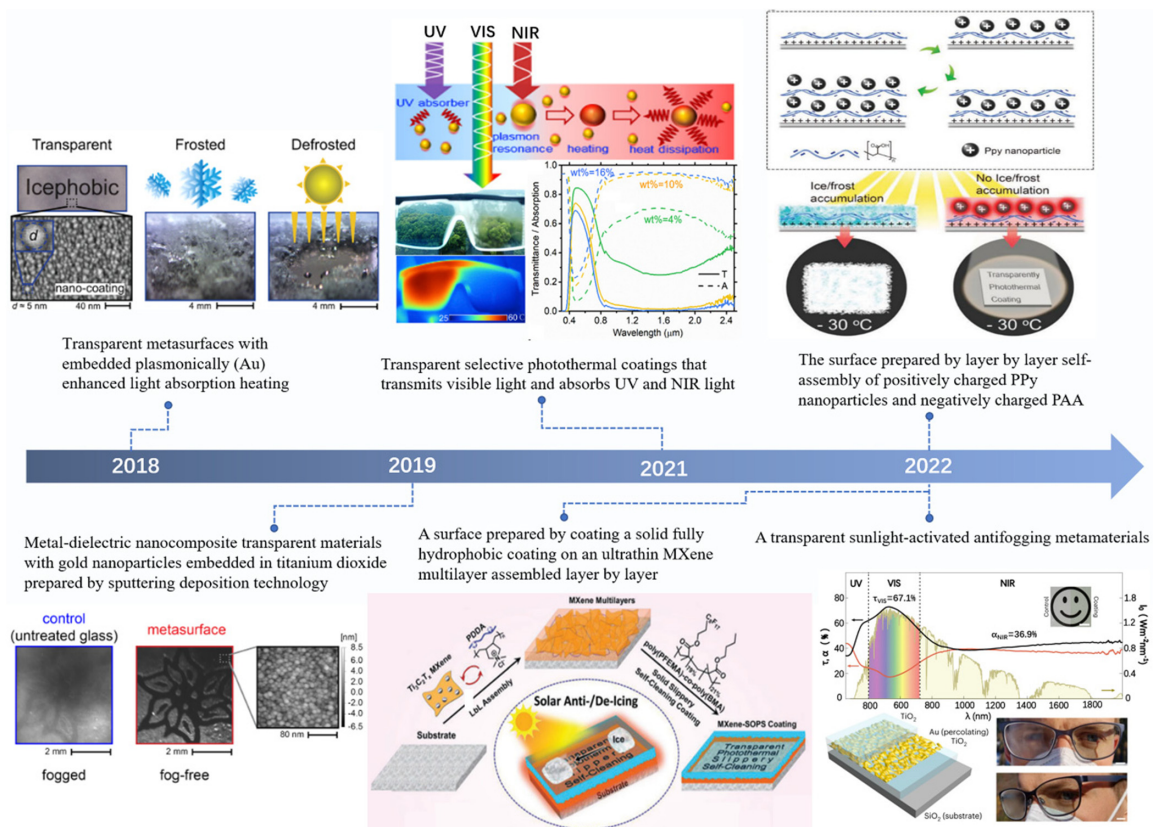


FIG. 7. Progress of transparent photothermal deicing coatings in the recent five years. Fabricating the transparent metasurfaces which is a nanocomposite of gold and titanium dioxide.¹⁰¹ The researcher proposes metal-dielectric nanocomposite transparent materials with gold nanoparticles embedded in titanium dioxide prepared by sputtering deposition technology.¹⁰² Li *et al.* developed a highly transparent, photothermally selective coating.¹⁰³ Transparent, photothermal, and icephobic surfaces via layer-by-layer assembly.¹⁰⁴ LBL-constructed ultrathin MXene multilayers can have a solid (i.e., liquid-free) omniphobic slippery (SOPS) coating put on top of them to create a highly transparent, scaleable solar anti-/de-icing surface.¹⁰⁵ An ultrathin passive metamaterial coating was constructed by sandwiching gold nanofilm between two dielectric TiO₂ nanolayers.¹⁰⁷ Reproduced with permission from Mitridis *et al.*, ACS Nano **12**, 7009–7017 (2018). Copyright 2018 American Chemical Society. Reproduced with permission from Walker *et al.*, Nano Lett. **19**, 1595–1604 (2019). Copyright 2019 American Chemical Society. Reproduced with permission from Li *et al.*, Cell Rep. Phys. Sci. **2**, 100435 (2021). Copyright 2021 Author(s), licensed under a Creative Commons Attribution license. Reproduced with permission from Wu *et al.*, Adv. Sci. **9**, 2105986 (2022). Copyright 2022 Author(s), licensed under a Creative Commons Attribution license. Reproduced with permission from Niu *et al.*, Adv. Mater. **34**, e2108232 (2022). Copyright 2022 Wiley-VCH GmbH. Reproduced with permission from Haechler *et al.*, Nat. Nanotechnol. **18**, 137 (2022). Copyright 2022 Nature.

The remaining melted water has a high specific heat capacity and reflects sunlight, which can significantly reduce photothermal efficiency.⁷⁰ Therefore, it is necessary to remove the melted water in order to obtain a clean and dry surface. To address this issue, a combination of photothermal deicing with other methods is proposed. In the following part, we present several combined strategies that can complement the drawbacks of sole photothermal deicing.

1. Combination of photothermal and slippery strategies

A liquid layer that separates the ice and substrate surface could provide an anti-icing self-lubricating surface and limits ice adhesion to the substrate.^{108,109} The liquid layer can be either an oil lubrication layer or a water lubrication layer.¹¹⁰ Simulations have demonstrated that the anisotropic motion of dangling hydroxyl groups on the surface of ice can cause the hexagonal surface ice structure to melt and

break apart, forming a water lubrication layer at temperatures below 0 °C [Fig. 8(a)].¹¹¹ Therefore, newly formed ice can be easily removed by wind due to the lower friction provided by the lubricant layer. It is important to note that the effectiveness of the water lubricant layer is limited by its temperature range, and below a certain temperature, the layer may freeze, causing an increase in ice adhesion strength.¹¹²

Slippery liquid-infused porous surfaces (SLIPS) use an organic lubricant that is trapped within a microstructure, polymer, or porous matrix material to create a smooth liquid surface with ultra-low ice adhesion strength, as shown in Fig. 8(b).^{109,113} Figure 8(c) shows the fabrication process of a SLIPS system.¹¹⁴ By combining photothermal and slippery strategies, both active and passive anti-icing materials work together to effectively melt frost/ice and prevent ice from sticking, respectively [as shown in Fig. 8(d)].¹¹⁵ For instance, Zhang *et al.* developed a smooth porous surface that consists of amino-functionalized Fe₃O₄ nanoparticles in a cross-linked network of

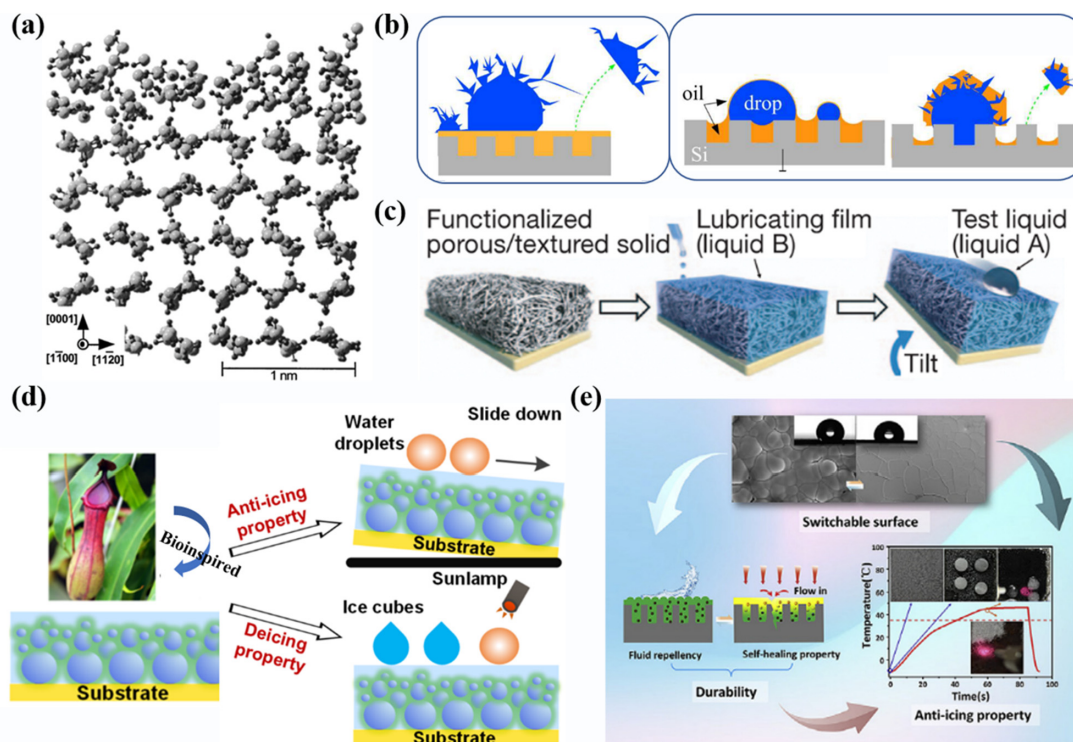


FIG. 8. (a) Molecular dynamics calculations have revealed a layer of ice that is melting;¹¹¹ (b) schematics showing two different mechanisms of frost formation and defrosting on a self-lubricating surface;¹⁰⁹ (c) a functionalized porous/textured solid is infiltrated with a low surface-energy, chemically inert liquid during the SLIPS fabrication process to create a physically smooth and chemically uniform lubricating layer on the substrate's surface;¹¹⁴ (d) multifunctional bioinspired photothermal slippery surface with low ice adhesion;¹¹⁶ and (e) to quickly defrost ice buildup and decrease frost accumulation, a sturdy lubricant-infused surface with photothermal responsiveness and reversible solid/liquid transformation was created.¹¹⁷ Panel (a) reproduced with permission from Ikeda-Fukazawa *et al.*, *J. Chem. Phys.* **120**, 1395–1401 (2004). Copyright 2004 AIP Publishing LLC. Panel (b) reproduced with permission from Rykaczewski *et al.*, *Langmuir* **29**, 5230–5238 (2013). Copyright 2013 American Chemical Society. Panel (c) reproduced with permission from Wong *et al.*, *Nature* **477**, 443–447 (2011). Panel (d) reproduced with permission from Zhang *et al.*, *Langmuir* **34**, 4052–4058 (2018). Copyright 2018 American Chemical Society. Panel (e) reproduced with permission from Wu *et al.*, *Mater. Des.* **185**, 108236 (2020). Copyright 2020 Elsevier Ltd.

poly(ethylene glycol methyl ether methacrylate-co-glycidyl methacrylate). The surface was infused with polyols and showed excellent active photothermal deicing performance. The adhesion strength of ice on the surface permeated by polyols is dramatically reduced, reaching an ultra-low value of 0.1 kPa [Fig. 8(d)].¹¹⁶ The lubricant can occasionally move from the wetting ridge and substrate structure to the frozen droplet surface, driven by capillary forces [Fig. 8(b), right], which could result in the lubricant being consumed during deicing or defrosting cycles. However, lubricant depletion would reduce the coating's durability and long-term ice resistance. Moreover, the environmental pollution associated with organic lubricant depletion cannot be ignored.¹¹² The superior water-repellent and deicing qualities of lubricant-infused surfaces are due in part to the high mobility and low surface energy of liquid lubricants, but these same characteristics also cause the lubricant to deplete in the presence of external shocks. To improve the long-term stability of the liquid-infused surface, Wu *et al.* proposed a concept of a solid-liquid switchable hydrophobic/smooth lubricant by injecting a low melting point cocoa butter lubricant and Fe₃O₄ nanoparticles into porous anodized aluminum oxide substrates.¹¹⁷ The Fe₃O₄ nanoparticles release heat through the photothermal effect, melting the solid lubricant into a smooth liquid surface

with high hydrophobicity. The self-healing property of the lubricant and the durability in the solid state synergistically diminish the loss of lubricant and enhance the long-term stability of lubricant-infused surfaces, as shown in Fig. 8(e).

2. Combination of photothermal and superhydrophobic strategies

Superhydrophobic surfaces (SHSs) with nano/microstructures can remove water droplets during the condensation phase by delaying ice nucleation and reducing ice accumulation.^{118–120} However, during some deicing processes, the freezing water can damage the substrate surface texture by partially penetrating the ice sheets and the substrate surface structures, as shown in Fig. 9(a).¹²¹ In contrast, photothermal superhydrophobic surfaces (PSHSs) employ a synergistic effect of photothermal conversion and superhydrophobicity.^{122,123} These surfaces can effectively absorb and convert sunlight into heat energy during the day, increasing the surface temperature to melt the ice.^{124,125} Again, the remaining melted water that stays at the surface would decrease the efficiency of photothermal conversion, as developed PSHSs can immediately remove the melted water, thus demonstrating self-

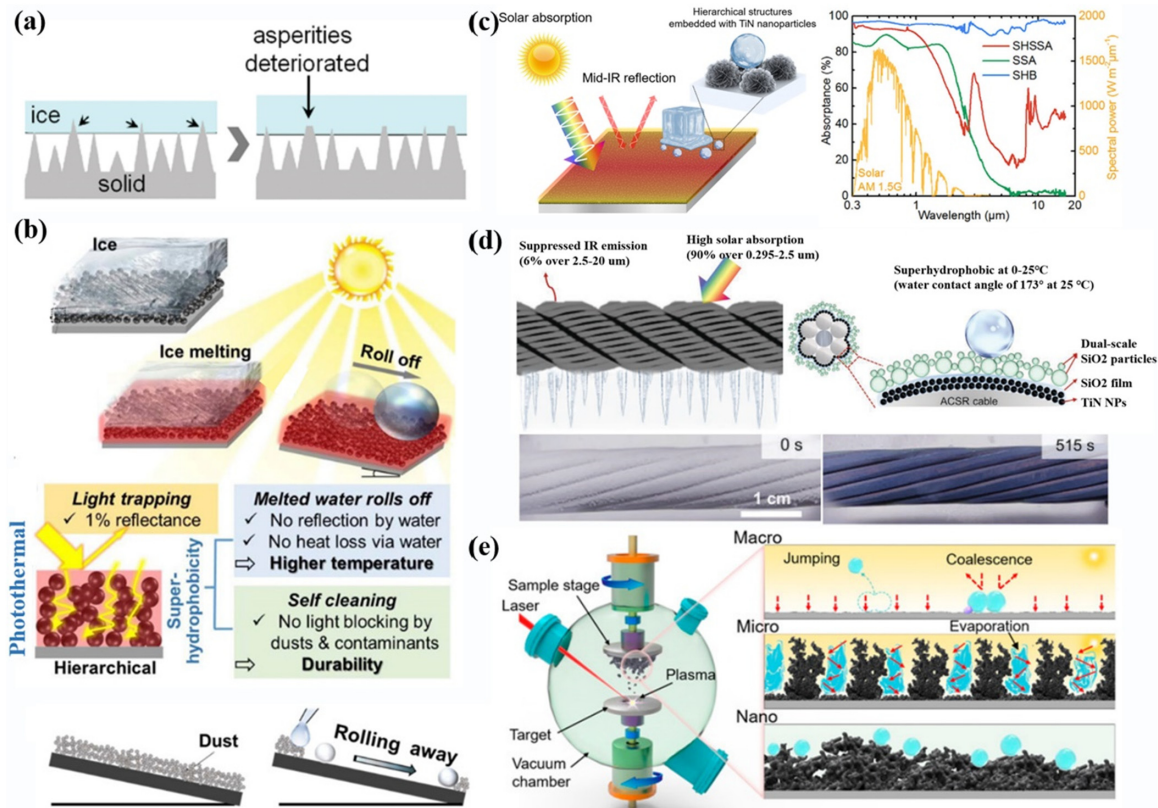


FIG. 9. (a) The presence of ice on superhydrophobic surfaces (left). The micro–nano structure will be destroyed in the repeated icing and deicing cycles due to the tip penetration (right).¹²¹ (b) Schematic of the photothermal superhydrophobic icephobic surface.⁷⁰ (c) Schematic of the superhydrophobic selective solar absorber (SHSSA).¹²⁸ (d) A low emissivity photothermal superhydrophobic coating compatible with flat surfaces and complex surfaces.¹³⁰ (e) Photothermal icephobic surfaces with self-removal of condensation due to self-propelling droplet transitions in extreme environments.⁷⁹ Panel (a) reproduced with permission from Lv *et al.*, ACS Nano 8, 3152–3169 (2014). Copyright 2014 American Chemical Society. Panel (c) reproduced with permission from Ma *et al.*, Cell Rep. Phys. Sci. 2, 100384 (2021). Copyright 2021 Author(s), licensed under a Creative Commons Attribution. Panel (d) reproduced with permission from Li *et al.*, Adv. Funct. Mater. 32, 2113297 (2022). Copyright 2022 Wiley-VCH.

cleaning properties. Moreover, rain or molten water can wash away dust and other pollutants to prevent blocking and scattering [Fig. 9(b)].^{70,126,127}

To date, most of the reported PSHSs used nearly black materials. While such materials are effective at absorbing sunlight, they tend to lose a lot of thermal radiation in the mid-infrared range, which reduces overall efficiency in converting solar energy into usable heat. As shown in Fig. 9(c), Ma *et al.* fabricated a low-cost selectively absorbing photothermal surface that is superhydrophobic by embedding titanium nitride (TiN) photothermal nanoparticles onto etched aluminum surfaces with micro/nanostructures. They obtained a high solar absorption rate (90%) and low infrared emissivity (42%) through a low surface energy treatment, which greatly reduced radiant heat loss and led to highly efficient solar-thermal energy conversion.¹²⁸ The icephobicity of such PSHSs has only been demonstrated on flat planes, leaving an open question on whether PSHSs could be applied to other complex curved surfaces, i.e., overhead lines.¹²⁹ Recently, Li *et al.* presented a solar-assisted superhydrophobic nano-coating with low emissivity that is compatible with both flat and complex curved surfaces. The work demonstrated the accumulated ice could be successfully

removed from the coated power line cables at -15°C , as shown in Fig. 9(d).¹³⁰

Under extreme conditions such as very low temperatures and high humidity, the loss of superhydrophobicity during deicing causes the ice to seep into the surface roughness, increasing the adhesion strength of the ice.⁷⁶ This leads to a reduced photothermal conversion efficiency. Zhang *et al.* created an efficient condensate self-removing solar anti-icing/frosting surface (CR-SAS) inspired by wheat leaves using ultrafine pulsed laser deposition. Through mutual water droplet coalescence, the condensate self-removal ensures a continuous dry area for light absorption and light-to-heat conversion, making CR-SAS an excellent solar anti-icing material under cold and humid conditions, as demonstrated in Fig. 9(e).⁷⁹

3. Combination of photothermal and phase-change strategies

Icephobic systems that completely rely on solar energy are interrupted during the night. This challenge has motivated the investigation of the incorporation of phase change materials (PCMs) into

photothermal materials, which offers a promising method for continuous anti-icing and deicing. The incorporation of encapsulated PCM (EPCM) can form surface protrusions that increase the surface roughness, endowing the surface with hydrophobicity or even superhydrophobicity for anti-icing. Furthermore, the phase transition of the EPCM during icing can cause a volume change, leading to the release of latent heat and generating local shear stress on the surface. This can result in a decrease in ice adhesion strength, as illustrated in Fig. 10(a).¹³¹

An effective combination of PCMs and photoresponsive materials can integrate photothermal conversion, energy storage, and heat release.¹³² In the presence of sunlight, photothermal materials initiate the light-to-heat conversion, raising the temperature to a higher value than the transition temperature of the PCM. Then, the PCM absorbs significant heat energy through its phase change and stores it as latent heat. In the absence of sunlight, the temperature drops considerably below the transition temperature of the PCM, the stored heat energy gradually releasing for zero-light deicing purposes. This cycle of energy

conversion, storage, and release is repeated each time sunlight is present or absent [Fig. 10(b)].¹³³ Continued researches are looking for an appropriate composite PCM since their applications are severely restricted by intrinsic characteristics such as low thermal conductivity.

Porous PCMs show excellent temperature control performance, good thermal conductivity, and high energy storage density, therefore effectively achieving thermal management [Fig. 10(c)].¹³⁴ For example, Sheng *et al.* reported a solar phase change material (SPCM) composed of expanded graphite (EG) and PDMS.¹³⁵ The EG is treated at high temperatures to create porous structures and a large surface area, and then the PCM (tetracethane) is infiltrated into it using the vacuum adsorption method to form a composite material. This is then introduced into a PDMS matrix to produce the SPCM, which can remain ice-free for 6 h after sunset [Fig. 10(d)]. Phase change material microcapsule is another form of PCM [Fig. 10(e)].¹³⁶ The integration of a phase change microcapsule layer with a superhydrophobic photothermal layer (SPT) has been successfully developed to provide whole-day anti-icing performance [Fig. 10(f)]. Specifically, the energy stored by

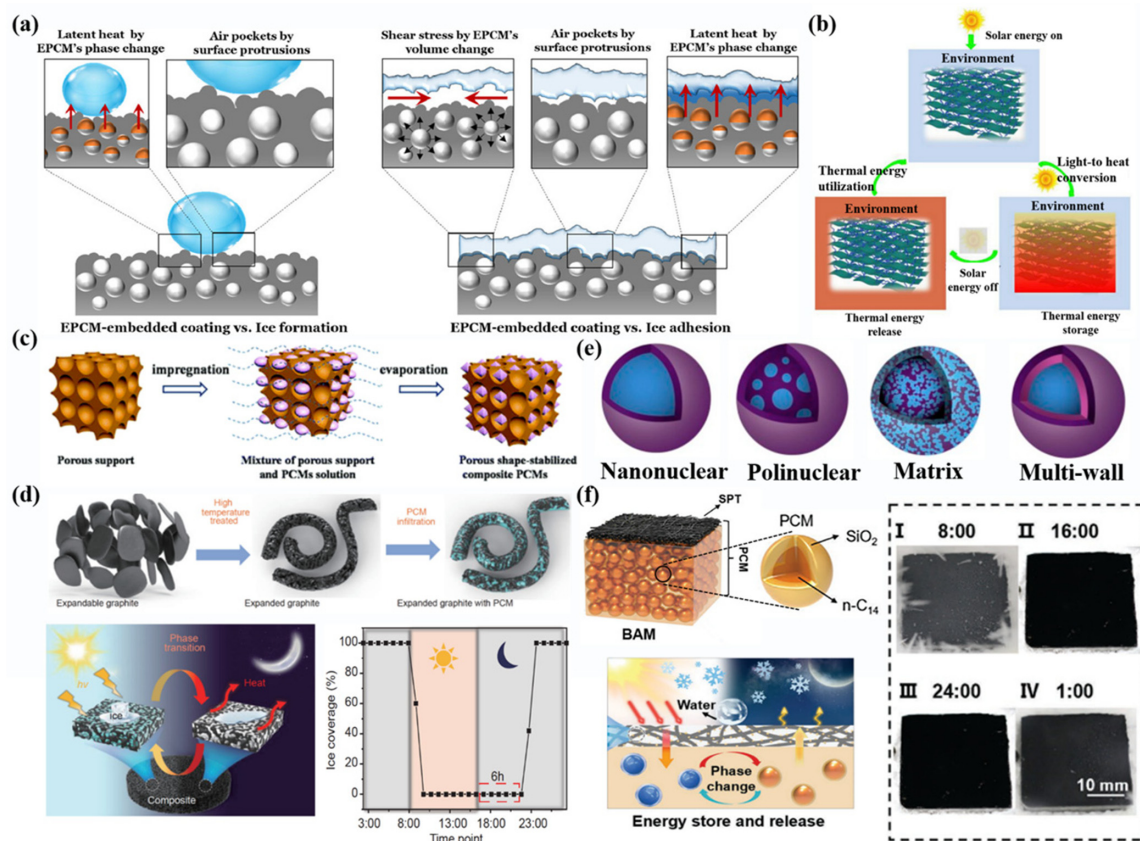


FIG. 10. (a) Mechanism diagram of phase change materials for anti-icing applications;¹³¹ (b) schematic diagram of the concept of light-to-heat conversion and storage of PCM;¹³³ (c) preparation scheme of porous-based composite PCMs using a two-step method;¹³⁴ (d) sustainable photothermal anti-icing material prepared by porous material filled with phase change agent;¹³⁵ (e) morphology of different types of microcapsules;¹³⁶ and (f) photothermal phase change microcapsules for deicing.¹³⁷ Panel (a) reproduced with permission from Ma *et al.*, *J. Energy Storage* **31**, 101638 (2020). Copyright 2020 Author(s), licensed under a Creative Commons Attribution. Copyright 2020 Elsevier. Panel (b) reproduced with permission from Lin *et al.*, *Sol. Energy Mater. Sol. Cells* **206**, 110229 (2020). Copyright 2020 Elsevier. Panel (c) reproduced with permission from Chen *et al.*, *Energy Environ. Sci.* **13**, 4498–4535 (2020). Copyright 2020 Elsevier. Panel (e) reproduced with permission from Jurkowska *et al.*, *Appl. Therm. Eng.* **98**, 365–373 (2016). Copyright 2016 Elsevier Ltd.

PCM is released at night, effectively preventing ice accumulation, while the SPT layer can subsequently remove water droplets promptly, delaying the formation of an ice layer.¹³⁷

4. Combination of photothermal and electrothermal strategies

Although the combination of photothermal material and PCMs can provide deicing performance at night, the low energy storage capacity of PCMs makes it difficult to maintain high efficiency throughout the period.¹¹² Electrothermal deicing is the most commonly used strategy for ice removal despite its high energy consumption and cost. Combining the photothermal and electrothermal strategies can largely mitigate these limitations, as shown in Figs. 11(a₁) and 11(b₁). Zhou's group reported the fabrication of a Ti₃C₂ MXene/Nanocellulose composite film [Fig. 11(a₂)] which is capable of electrothermal and photothermal heating.¹³⁸ It has good performance in low-pressure driven joule heating and photoresponsive heating, proving the feasibility of efficient thermal deicing under practical conditions. In Fig. 11(b₁), the electrothermal anti-icing mode is turned on at night, while the photothermal anti-icing mode is switched on during the day, resulting in an ice-free film throughout the whole day.¹³⁹ Figure 11(b₂) shows a porous photo-electro-thermal PDMS/polypyrrole (PPy) membrane that can be used for all-day anti-icing/deicing applications. The unique hierarchical structure provides more traps for incoming light and thus yields outstanding broadband solar absorption, causing the membrane to remain ice-free all day long due to the combined photothermal and electrothermal effects.¹⁴⁰ Adding solar panels to the system enables the electrothermal anti-icing model to be powered in the absence of an external power source and consume less power, making the combined strategy more practical in the long run.¹⁴¹

5. Combination of photothermal and other strategies

The most effective anti-icing strategies in the future should ideally demonstrate optimal performance in various conditions. To achieve this, in addition to the aforementioned common photothermal+ strategies, several other combination strategies are reviewed as well. For instance, Dash *et al.* reported a photothermal trap applied on a substrate as a laminate, which consists of three mutually complementary layers, i.e., a selective absorber of solar radiation, a thermal spreader that disperses heat laterally, and an insulating layer that reduces lateral heat loss [Fig. 12(a)].⁷⁶ Another notable anti-icing coating developed recently utilizes patterned hydrogel encapsulated ice nucleating proteins (PHINPs) to localize the ice nucleation on top of the gel, as shown in Fig. 12(b). These PHINPs were patterned on a photothermal polypyrrole surface, and the composite coating has shown high anti-icing performance during the whole day.¹⁴²

Amphiphilic materials have bifunctional properties: hydrophobic groups reduce the contact area between water and substrate, while hydrophilic groups lower the freezing point of water. Consequently, amphiphilic materials have potential use in deicing applications, as shown in Fig. 12(c₁).¹⁴³ A coating with extremely low ice shear stress has been designed by combining photoresponsive carbon nanofibers and an amphiphilic material integrated with hydrophobic PDMS and hydrophilic PVP [Fig. 12(c₂)].¹⁴⁴ To conclude, using the photothermal effect alone is insufficient to prevent freezing in complex circumstances, and combining photothermal effects with other deicing methods is highly desired for practical and flexible applications.

VII. CONCLUSIONS AND PROSPECTS

In summary, we have given an overview of the progress of various coatings that are massively employed in photothermal deicing and survey design strategies for photothermal materials and structures.

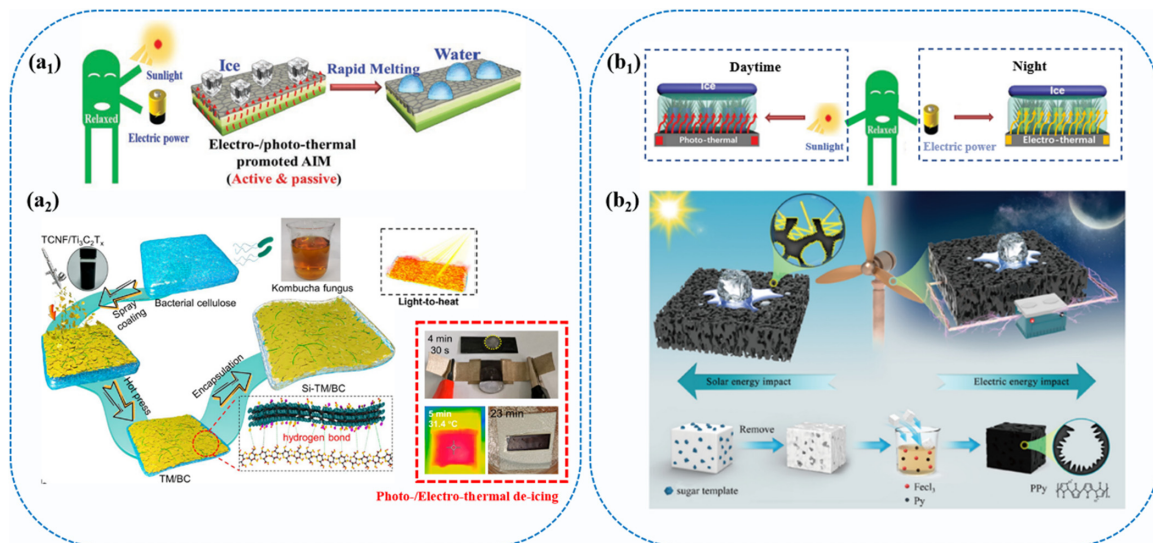


FIG. 11. (a₁) Schematic of the concept of photothermal or electrothermal acting on deicing;¹³⁹ (a₂) the multifunctional films with outstanding electro-/photothermal deicing performance;¹³⁸ (b₁) schematic of the concept of all-day continuous icephobic electro-photo-thermal membrane;¹³⁹ and (b₂) all-day available photo-electro-thermal film based on PDMS/PPy hierarchical structure.¹⁴⁰ Panel (a₁) reproduced with permission from He *et al.*, *Adv. Mater. Interfaces* **9**, 2200275 (2022). Copyright 2022 Wiley-VCH. Panel (a₂) reproduced with permission from Zhou *et al.*, *ACS Nano* **15**, 12405–12417 (2021). Copyright 2021 American Chemical Society. Panel (b₁) reproduced with permission from He *et al.*, *Adv. Mater. Interfaces* **9**, 2200275 (2022). Copyright 2022 Wiley-VCH.

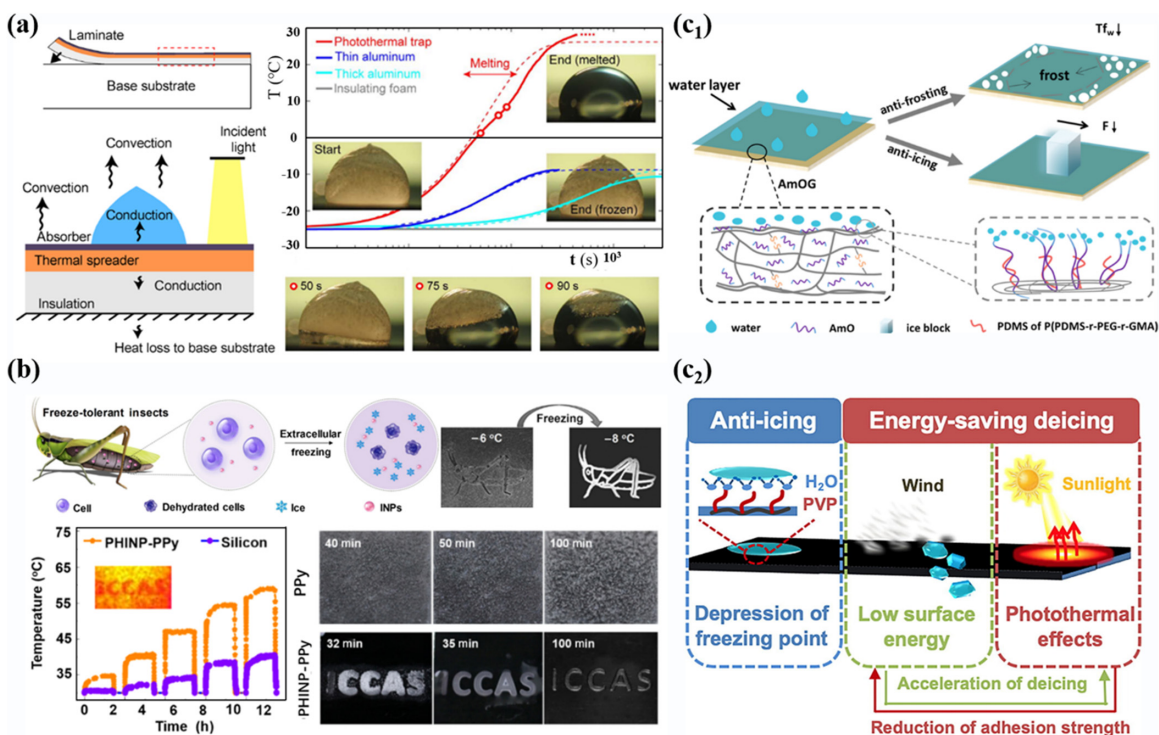


FIG. 12. (a) A highly efficient photothermal trap to prevent ice accumulation, which is composed of a light absorption layer, heat transfer layer, and thermal insulation layer;⁷⁶ (b) the photothermal hydrogel encapsulated antifreeze protein maintains efficient deicing at any time of day;¹⁴² (c₁) amphiphilic organic gel shows great potential in anti-icing applications;¹⁴³ and (c₂) a sunlight-responsive amphiphilic material for ice mitigation.¹⁴⁴ Panel (a) reproduced with permission from Dash *et al.*, *Sci. Adv.* **4**, eaat0127 (2018). Copyright 2018 Science Advance. Panel (c₁) reproduced with permission from Yu *et al.*, *ACS Appl. Mater. Interfaces* **11**, 12838–12845 (2019). Copyright 2019 American Chemical Society. Panel (c₂) reproduced with permission from Guo *et al.*, *Chem. Eng. J.* **402**, 126161 (2020). Copyright 2020 Elsevier.

Photothermal heating is advantageous compared to traditional deicing methods due to its low cost, environmental friendliness, and sustainability. Choosing the appropriate photothermal conversion materials is crucial to the effectiveness of photothermal deicers. Light-trapping structures can improve solar energy absorption but may compromise transparency to some extent. Selective solar absorption coatings are a promising solution to balance visual transparency and photothermal performance, requiring high absorption in the solar infrared spectrum (0.75–2.5 μm) and high transmittance in the visible band (0.38–0.75 μm). To address the limitations of photothermal deicing in complex environments, photothermal+ strategies have been developed to enhance deicing efficiency and create the next generation of photothermal materials.

Although great gratifying progress has been made in laboratory photothermal deicing, challenges remain, and there are key points ahead for future research. First, while current techniques focus on the integration of various photothermal materials with high photothermal absorption and photothermal efficiency, the risk of overheating temperature poses a significant danger. Therefore, the design of photothermal coatings that can automatically dissipate heat along with ambient environments variation is encouraged. Second, practical photothermal effects are subject to constantly varying sunlight intensity and position, which laboratory measurements often fail to account for, as they typically only consider a fixed position (perpendicular to the surface) and

a constant intensity (1 kW m^{-2}). Therefore, it is imperative to investigate the photothermal icephobic surface under weaker light intensity. These explorations in the future will speed up the development of photothermal deicing in practical applications.

ACKNOWLEDGMENTS

The work was supported by the National Key Research and Development Program of China (No. 2020YFE0100300) and the Chinese National Nature Science Foundation (No. 22122206).

AUTHOR DECLARATIONS

Conflict of Interest

The authors have no conflicts to disclose.

Author Contributions

Tongtong Hao: Conceptualization (equal); Data curation (equal); Formal analysis (equal); Investigation (equal); Methodology (equal); Project administration (equal); Resources (equal); Software (equal); Supervision (equal); Validation (equal); Visualization (equal); Writing – original draft (equal); Writing – review & editing (equal). **Dan Wang:** Conceptualization (supporting); Data curation (equal); Formal analysis (supporting); Investigation (lead); Methodology (equal);

Visualization (equal); Writing – original draft (supporting); Writing – review & editing (supporting). **Xiaoting Chen:** Conceptualization (supporting); Writing – review & editing (supporting). **Abdullatif Jazzar:** Conceptualization (supporting); Data curation (supporting); Investigation (supporting); Visualization (supporting); Writing – original draft (supporting); Writing – review & editing (supporting). **Pengju Shi:** Conceptualization (supporting); Data curation (supporting); Investigation (supporting); Visualization (supporting); Writing – original draft (supporting); Writing – review & editing (supporting). **Cunyi Li:** Conceptualization (supporting). **Heran Wang:** Visualization (supporting). **Ximin He:** Conceptualization (equal); Methodology (equal); Writing – original draft (equal); Writing – review & editing (equal). **Zhiyuan He:** Conceptualization (lead); Data curation (equal); Formal analysis (equal); Investigation (equal); Methodology (equal); Project administration (equal); Resources (equal); Supervision (lead); Validation (equal); Visualization (equal); Writing – original draft (lead).

DATA AVAILABILITY

Data sharing is not applicable to this article as no new data were created or analyzed in this study.

REFERENCES

- ¹O. Parent and A. Ilinca, *Cold Reg. Sci. Technol.* **65**, 88–96 (2011).
- ²C. C. Ryerson, *Cold Reg. Sci. Technol.* **65**, 97–110 (2011).
- ³N. Dalili, A. Edrissy, and R. Carriveau, *Renewable Sustainable Energy Rev.* **13**, 428–438 (2009).
- ⁴O. Fakorede, Z. Feger, H. Ibrahim, A. Ilinca, J. Perron, and C. Masson, *Renewable Sustainable Energy Rev.* **65**, 662–675 (2016).
- ⁵P.-O. A. Borrebaek, B. P. Jelle, and Z. Zhang, *Sol. Energy Mater. Sol. Cells* **206**, 110306 (2020).
- ⁶T. Wang, Y. Zheng, A.-R. O. Raji, Y. Li, W. K. A. Sikkema, and J. M. Tour, *ACS Appl. Mater. Interfaces* **8**, 14169–14173 (2016).
- ⁷D. M. Ramakrishna and T. Viraraghavan, *Water, Air, Soil Pollut.* **166**, 49–63 (2005).
- ⁸T. Oki and S. Kanae, *Science* **313**, 1068–1072 (2006).
- ⁹N. S. Lewis, *Science* **315**, 798–801 (2007).
- ¹⁰V. H. Dalvi, S. V. Panse, and J. B. Joshi, *Nat. Clim. Change* **5**, 1007–1013 (2015).
- ¹¹H.-Y. Chen, Y.-F. Xu, D.-B. Kuang, and C.-Y. Su, *Energy Environ. Sci.* **7**, 3887–3901 (2014).
- ¹²H. Chen, L. Shao, T. Ming, Z. Sun, C. Zhao, B. Yang, and J. Wang, *Small* **6**, 2272–2280 (2010).
- ¹³F. Zhao, Y. Guo, X. Zhou, W. Shi, and G. Yu, *Nat. Rev. Mater.* **5**, 388–401 (2020).
- ¹⁴H. Yu, Y. Peng, Y. Yang, and Z.-Y. Li, *npj Comput. Mater.* **5**, 45 (2019).
- ¹⁵J. Wang, Y. Li, L. Deng, N. Wei, Y. Weng, S. Dong, D. Qi, J. Qiu, X. Chen, and T. Wu, *Adv. Mater.* **29**, 1603730 (2017).
- ¹⁶F. Meng, B. Ju, S. Zhang, and B. Tang, *J. Mater. Chem. A* **9**, 13746–13769 (2021).
- ¹⁷N. S. Fuzil, N. H. Othman, N. H. Alias, F. Marpani, M. H. D. Othman, A. F. Ismail, W. J. Lau, K. Li, T. D. Kusworo, I. Ichinose, and M. M. A. Shirazi, *Desalination* **517**, 115259 (2021).
- ¹⁸M. Gao, C. K. Peh, F. L. Meng, and G. W. Ho, *Small Methods* **5**, 2001200 (2021).
- ¹⁹X. Wu, G. Y. Chen, G. Owens, D. Chu, and H. Xu, *Mater. Today Energy* **12**, 277–296 (2019).
- ²⁰Q. Zhang, W. Xu, and X. Wang, *Sci. China Mater.* **61**, 905–914 (2018).
- ²¹C. Wang, Y. Wang, X. Jiang, J. Xu, W. Huang, F. Zhang, J. Liu, F. Yang, Y. Song, Y. Ge, Q. Wu, M. Zhang, H. Chen, J. Liu, and H. Zhang, *Adv. Opt. Mater.* **7**, 1900060 (2019).
- ²²X. Wang, Q. Liu, S. Wu, B. Xu, and H. Xu, *Adv. Mater.* **31**, e1807716 (2019).
- ²³K. Bae, G. Kang, S. K. Cho, W. Park, K. Kim, and W. J. Padilla, *Nat. Commun.* **6**, 10103 (2015).
- ²⁴E. Garnett and P. Yang, *Nano Lett.* **10**, 1082–1087 (2010).
- ²⁵N. Li, Y. Zhang, H. Zhi, J. Tang, Y. Shao, L. Yang, T. Sun, H. Liu, and G. Xue, *Chem. Eng. J.* **429**, 132183 (2022).
- ²⁶P. Fan, B. Bai, M. Zhong, H. Zhang, J. Long, J. Han, W. Wang, and G. Jin, *ACS Nano* **11**, 7401–7408 (2017).
- ²⁷Z. Yin, H. Wang, M. Jian, Y. Li, K. Xia, M. Zhang, C. Wang, Q. Wang, M. Ma, Q. S. Zheng, and Y. Zhang, *ACS Appl. Mater. Interfaces* **9**, 28596–28603 (2017).
- ²⁸P. Zhang, J. Li, L. Lv, Y. Zhao, and L. Qu, *ACS Nano* **11**, 5087–5093 (2017).
- ²⁹H. Ren, M. Tang, B. Guan, K. Wang, J. Yang, F. Wang, M. Wang, J. Shan, Z. Chen, D. Wei, H. Peng, and Z. Liu, *Adv. Mater.* **29**, 1702590 (2017).
- ³⁰Y. Li, C. Lin, Z. Wu, Z. Chen, C. Chi, F. Cao, D. Mei, H. Yan, C. Y. Tso, C. Y. H. Chao, and B. Huang, *Adv. Mater.* **33**, 2005074 (2021).
- ³¹H. Li, Y. Li, J. Wu, X. Jia, J. Yang, D. Shao, L. Feng, S. Wang, and H. Song, *ACS Appl. Mater. Interfaces* **14**, 29302–29314 (2022).
- ³²Y. Zhao, C. Yan, T. Hou, H. Dou, and H. Shen, *ACS Appl. Mater. Interfaces* **14**, 26077–26087 (2022).
- ³³X. Ji, Y. Jiang, T. Liu, S. Lin, and A. Du, *Cell Rep. Phys. Sci.* **3**, 100815 (2022).
- ³⁴J. Hu, H. Li, Z. Liu, and G. Jiang, *Surf. Coat. Technol.* **425**, 127646 (2021).
- ³⁵G. Jiang, L. Chen, S. Zhang, and H. Huang, *ACS Appl. Mater. Interfaces* **10**, 36505–36511 (2018).
- ³⁶X. Fang, Y. Liu, S. Lei, C. Li, J. Ou, and A. Amirfazli, *RSC Adv.* **12**, 13792–13796 (2022).
- ³⁷M. L. Brongersma, N. J. Halas, and P. Nordlander, *Nat. Nanotechnol.* **10**, 25–34 (2015).
- ³⁸M. Lisowski, P. Loukakos, U. Bovensiepen, J. Stähler, C. Gahl, and M. Wolf, *Phys. Rev. Lett.* **78**, 165–176 (2004).
- ³⁹C. Chen, Y. Kuang, and L. Hu, *Joule* **3**, 683–718 (2019).
- ⁴⁰M. Ahlwat, D. Mittal, and V. Govind Rao, *Commun. Mater.* **2**, 114 (2021).
- ⁴¹P. Cheng, D. Wang, and P. Schaaf, *Adv. Sustainable Syst.* **6**, 2200115 (2022).
- ⁴²Y. Liu, J. Zhao, S. Zhang, D. Li, X. Zhang, Q. Zhao, and B. Xing, *Environ. Sci.: Nano* **9**, 2264–2296 (2022).
- ⁴³L. Xiao, X. Chen, X. Yang, J. Sun, and J. Geng, *ACS Appl. Polym. Mater.* **2**, 4273–4288 (2020).
- ⁴⁴H. Wang, C. Zhang, B. Zhou, Z. Zhang, J. Shen, and A. Du, *Adv. Compos. Hybrid Mater.* **2**, 743–752 (2019).
- ⁴⁵H. Wang, A. Du, X. Ji, C. Zhang, B. Zhou, Z. Zhang, and J. Shen, *ACS Appl. Mater. Interfaces* **11**, 42057–42065 (2019).
- ⁴⁶W. Sun, A. Du, Y. Feng, J. Shen, S. Huang, J. Tang, and B. Zhou, *ACS Nano* **10**, 9123–9128 (2016).
- ⁴⁷W. Guan, Y. Guo, and G. Yu, *Small* **17**, 2007176 (2021).
- ⁴⁸H. Lin, X. Wang, L. Yu, Y. Chen, and J. Shi, *Nano Lett.* **17**, 384–391 (2017).
- ⁴⁹R. Li, L. Zhang, L. Shi, and P. Wang, *ACS Nano* **11**, 3752–3759 (2017).
- ⁵⁰F. Shahzad, M. Alhabeab, C. B. Hatter, B. Anasori, S. Man Hong, C. M. Koo, and Y. Gogotsi, *Science* **353**, 1137–1140 (2016).
- ⁵¹X. Fan, L. Liu, X. Jin, W. Wang, S. Zhang, and B. Tang, *J. Mater. Chem. A* **7**, 14319–14327 (2019).
- ⁵²D. Xu, Z. Li, L. Li, and J. Wang, *Adv. Funct. Mater.* **30**, 2000712 (2020).
- ⁵³Z. Tang, H. Gao, X. Chen, Y. Zhang, A. Li, and G. Wang, *Nano Energy* **80**, 105454 (2021).
- ⁵⁴J. Lou-Franco, B. Das, C. Elliott, and C. Cao, *Nano-Micro Lett.* **13**, 10 (2020).
- ⁵⁵W. Kim, N. Kim, J. W. Park, and Z. H. Kim, *Nanoscale* **8**, 987–994 (2016).
- ⁵⁶L.-C. Cheng, J.-H. Huang, H. M. Chen, T.-C. Lai, K.-Y. Yang, R.-S. Liu, M. Hsiao, C.-H. Chen, L.-J. Her, and D. P. Tsai, *J. Mater. Chem.* **22**, 2244–2253 (2012).
- ⁵⁷M. Rycenga, M. R. Langille, M. L. Personick, T. Ozel, and C. A. Mirkin, *Nano Lett.* **12**, 6218–6222 (2012).
- ⁵⁸E. Ringe, C. J. DeSantis, S. M. Collins, M. Duchamp, R. E. Dunin-Borkowski, S. E. Skrabalak, and P. A. Midgley, *Sci. Rep.* **5**, 17431 (2015).
- ⁵⁹G. Baffou, R. Quidant, and C. Girard, *Phys. Rev. B* **82**, 165424 (2010).
- ⁶⁰F. Zhao, X. Zhou, Y. Shi, X. Qian, M. Alexander, X. Zhao, S. Mendez, R. Yang, L. Qu, and G. Yu, *Nat. Nanotechnol.* **13**, 489–495 (2018).
- ⁶¹P. Ying, B. Ai, W. Hu, Y. Geng, L. Li, K. Sun, S. C. Tan, W. Zhang, and M. Li, *Nano Energy* **89**, 106443 (2021).

- ⁶²P. Fan, H. Wu, M. Zhong, H. Zhang, B. Bai, and G. Jin, *Nanoscale* **8**, 14617–14624 (2016).
- ⁶³X. Liu, Y. Tian, F. Chen, Y. Mu, A. Caratenuto, M. L. Minus, and Y. Zheng, *J. Mater. Chem. A* **10**, 18657–18670 (2022).
- ⁶⁴Z. Xie, H. Wang, Y. Geng, M. Li, Q. Deng, Y. Tian, R. Chen, X. Zhu, and Q. Liao, *ACS Appl. Mater. Interfaces* **13**, 48308–48321 (2021).
- ⁶⁵S.-H. Lee, J. Kim, M. Seong, S. Kim, H. Jang, H. W. Park, and H. E. Jeong, *Compos. Sci. Technol.* **217**, 109086 (2022).
- ⁶⁶H. Joukhdar, A. Seifert, T. Jüngst, J. Groll, M. S. Lord, and J. Rnjak-Kovacina, *Adv. Mater.* **33**, 2100091 (2021).
- ⁶⁷B. Yu, Z. Sun, Y. Liu, Z. Zhang, Y. Wu, and F. Zhou, *ACS Appl. Mater. Interfaces* **13**, 37609–37616 (2021).
- ⁶⁸C. Wu, H. Geng, S. Tan, J. Lv, H. Wang, Z. He, and J. Wang, *Mater. Horiz.* **7**, 2097–2104 (2020).
- ⁶⁹H. Zhang, X. Xu, M. Wu, Y. Zhao, F. Sun, Q. Xin, Y. Zhou, M. Qin, Y. Zhou, C. Ding, and J. Li, *Adv. Funct. Mater.* **32**, 2201795 (2022).
- ⁷⁰S. Wu, Y. Du, Y. Alsaid, D. Wu, M. Hua, Y. Yan, B. Yao, Y. Ma, X. Zhu, and X. He, *Proc. Natl. Acad. Sci. U. S. A.* **117**, 11240–11246 (2020).
- ⁷¹Y. Gu, X. Mu, P. Wang, X. Wang, J. Liu, J. Shi, A. Wei, Y. Tian, G. Zhu, H. Xu, J. Zhou, and L. Miao, *Nano Energy* **74**, 104857 (2020).
- ⁷²H. Wang, C. Zhang, and A. Du, *Sol. RRL* **7**, 2201128 (2023).
- ⁷³E. S. Toberer, L. L. Baranowski, and C. Dames, *Annu. Rev. Mater. Res.* **42**, 179–209 (2012).
- ⁷⁴T. Niu, B. Zhou, Z. Zhang, X. Ji, J. Yang, Y. Xie, H. Wang, and A. Du, *Nanomater* **10**(12), 2527 (2020).
- ⁷⁵H. J. Xu, Z. B. Xing, F. Wang, and Z. J. Cheng, *Chem. Eng. Sci.* **195**, 462–483 (2019).
- ⁷⁶S. Dash, J. de Ruiter, and K. K. Varanasi, *Sci. Adv.* **4**, eaat0127 (2018).
- ⁷⁷H. Wang, C. Zhang, X. Ji, J. Yang, Z. Zhang, Y. Ma, Z. Zhang, B. Zhou, J. Shen, and A. Du, *ACS Appl. Mater. Interfaces* **14**, 10257–10266 (2022).
- ⁷⁸M. A. Jahid, J. Wang, E. Zhang, Q. Duan, and Y. Feng, *Energy Convers. Manage.* **263**, 115705 (2022).
- ⁷⁹H. Zhang, G. Zhao, S. Wu, Y. Alsaid, W. Zhao, X. Yan, L. Liu, G. Zou, J. Lv, X. He, Z. He, and J. Wang, *Proc. Natl. Acad. Sci. U. S. A.* **118**, e2100978118 (2021).
- ⁸⁰X. Y. Liu, *Adv. Cryst. Growth Res.* **2001**, 42–61.
- ⁸¹S. Sastry, *Nature* **438**, 746–747 (2005).
- ⁸²T. M. Schutzius, S. Jung, T. Maitra, P. Eberle, C. Antonini, C. Stamatopoulos, and D. Poulikakos, *Langmuir* **31**, 4807–4821 (2015).
- ⁸³L. Mishchenko, B. Hatton, V. Bahadur, J. A. Taylor, T. Krupenkin, and J. Aizenberg, *ACS Nano* **4**, 7699–7707 (2010).
- ⁸⁴T. M. Schutzius, S. Jung, T. Maitra, G. Graeber, M. Köhne, and D. Poulikakos, *Nature* **527**, 82–85 (2015).
- ⁸⁵Z. Zhang and X. Y. Liu, *Chem. Soc. Rev.* **47**, 7116–7139 (2018).
- ⁸⁶Y. Zhuo, J. Chen, S. Xiao, T. Li, F. Wang, J. He, and Z. Zhang, *Mater. Horiz.* **8**, 3266–3280 (2021).
- ⁸⁷G. Bai, D. Gao, Z. Liu, X. Zhou, and J. Wang, *Nature* **576**, 437–441 (2019).
- ⁸⁸H. Yang, C. Ma, K. Li, K. Liu, M. Loznik, R. Teeuwen, J. C. van Hest, X. Zhou, A. Herrmann, and J. Wang, *Adv. Mater.* **28**, 5008–5012 (2016).
- ⁸⁹L. Zhang, C. Tian, G. A. Waychunas, and Y. R. Shen, *J. Am. Chem. Soc.* **130**, 7686–7694 (2008).
- ⁹⁰Z. He, W. J. Xie, Z. Liu, G. Liu, Z. Wang, Y. Q. Gao, and J. Wang, *Sci. Adv.* **2**, e1600345 (2016).
- ⁹¹Y. Zhuo, S. Xiao, A. Amirfazli, J. He, and Z. J. Zhang, *Chem. Eng. J.* **405**, 127088 (2021).
- ⁹²Z. He, Y. Zhuo, Z. Zhang, and J. He, *Soft Matter* **11**, 1343 (2021).
- ⁹³K. Golovin, S. P. R. Kobaku, D. H. Lee, E. T. DiLoreto, J. M. Mabry, and A. Tuteja, *Sci. Adv.* **2**, e1501496 (2016).
- ⁹⁴K. A. Emelyanenko, A. M. Emelyanenko, and L. B. Boinovich, *Coatings* **10**, 648 (2020).
- ⁹⁵D. Chen, M. D. Gelenter, M. Hong, R. E. Cohen, and G. H. McKinley, *ACS Appl. Mater. Interfaces* **9**, 4202–4214 (2017).
- ⁹⁶Z. He, S. Xiao, H. Gao, J. He, and Z. Zhang, *Soft Matter* **13**, 6562–6568 (2017).
- ⁹⁷D. T. Papanastasiou, A. Schultheiss, D. Muñoz-Rojas, C. Celle, A. Carella, J. P. Simonato, and D. Bellet, *Adv. Funct. Mater.* **30**, 1910225 (2020).
- ⁹⁸M. Guo, L. Gao, Y. Wei, Y. Ma, Y. Jianyong, and B. Ding, *Sol. Energy Mater. Sol. Cells* **219**, 110796 (2021).
- ⁹⁹D. Yang, B. Zhou, G. Han, Y. Feng, J. Ma, J. Han, C. Liu, and C. Shen, *ACS Appl. Mater. Interfaces* **13**, 8909–8918 (2021).
- ¹⁰⁰X. Fan, Y. Ding, Y. Liu, J. Liang, and Y. Chen, *ACS Nano* **13**, 8124–8134 (2019).
- ¹⁰¹E. Mitridis, T. M. Schutzius, A. Sicher, C. U. Hail, H. Eghlidi, and D. Poulikakos, *ACS Nano* **12**, 7009–7017 (2018).
- ¹⁰²C. Walker, E. Mitridis, T. Kreiner, H. Eghlidi, T. M. Schutzius, and D. Poulikakos, *Nano Lett.* **19**, 1595–1604 (2019).
- ¹⁰³Y. Li, X. Wang, and J. Sun, *Chem. Soc. Rev.* **41**, 5998–6009 (2012).
- ¹⁰⁴S. Wu, Z. Liang, Y. Li, S. Chay, Z. He, S. Tan, J. Wang, X. Zhu, and X. He, *Adv. Sci.* **9**, 2105986 (2022).
- ¹⁰⁵W. Niu, G. Y. Chen, H. Xu, X. Liu, and J. Sun, *Adv. Mater.* **34**, e2108232 (2022).
- ¹⁰⁶W. Li, C. Lin, W. Ma, Y. Li, F. Chu, B. Huang, and S. Yao, *Cell Rep. Phys. Sci.* **2**, 100435 (2021).
- ¹⁰⁷I. Haechler, N. Ferru, G. Schnoering, E. Mitridis, T. M. Schutzius, and D. Poulikakos, *Nat. Nanotechnol.* **18**, 137 (2023).
- ¹⁰⁸R. Dou, J. Chen, Y. Zhang, X. Wang, D. Cui, Y. Song, L. Jiang, and J. Wang, *ACS Appl. Mater. Interfaces* **6**, 6998–7003 (2014).
- ¹⁰⁹K. Rykaczewski, S. Anand, S. B. Subramanyam, and K. K. Varanasi, *Langmuir* **29**, 5230–5238 (2013).
- ¹¹⁰S. Jiang, Y. Diao, and H. Yang, *Adv. Colloid Interface Sci.* **308**, 102756 (2022).
- ¹¹¹T. Ikeda-Fukazawa and K. Kawamura, *J. Chem. Phys.* **120**, 1395–1401 (2004).
- ¹¹²Z. He and J. Wang, *Innovation* **3**, 100278 (2022).
- ¹¹³H. F. Bohn and W. Federle, *Proc. Natl. Acad. Sci. U. S. A.* **101**, 14138–14143 (2004).
- ¹¹⁴T.-S. Wong, S. H. Kang, S. K. Y. Tang, E. J. Smythe, B. D. Hatton, A. Grinthal, and J. Aizenberg, *Nature* **477**, 443–447 (2011).
- ¹¹⁵X. Yin, Y. Zhang, D. Wang, Z. Liu, Y. Liu, X. Pei, B. Yu, and F. Zhou, *Adv. Funct. Mater.* **25**, 4237–4245 (2015).
- ¹¹⁶G. Zhang, Q. Zhang, T. Cheng, X. Zhan, and F. Chen, *Langmuir* **34**, 4052–4058 (2018).
- ¹¹⁷D. Wu, L. Ma, F. Zhang, H. Qian, B. Minhas, Y. Yang, X. Han, and D. Zhang, *Mater. Des.* **185**, 108236 (2020).
- ¹¹⁸X. Yao, Y. Song, and L. Jiang, *Adv. Mater.* **23**, 719–734 (2011).
- ¹¹⁹T. Sun, L. Feng, X. Gao, and L. Jiang, *Acc. Chem. Res.* **38**, 644–652 (2005).
- ¹²⁰A. Alizadeh, V. Bahadur, A. Kulkarni, M. Yamada, and J. A. Ruud, *MRS Bull.* **38**, 407–411 (2013).
- ¹²¹J. Lv, Y. Song, L. Jiang, and J. Wang, *ACS Nano* **8**, 3152–3169 (2014).
- ¹²²C.-H. Xue, H.-G. Li, X.-J. Guo, Y.-R. Ding, B.-Y. Liu, Q.-F. An, and Y. Zhou, *Chem. Eng. J.* **424**, 130553 (2021).
- ¹²³H. Xie, W.-H. Xu, Y. Du, J. Gong, R. Niu, T. Wu, and J.-P. Qu, *Small* **18**, 2200175 (2022).
- ¹²⁴B. Wu, X. Cui, H. Jiang, N. Wu, C. Peng, Z. Hu, X. Liang, Y. Yan, J. Huang, and D. Li, *J. Colloid Interface Sci.* **590**, 301–310 (2021).
- ¹²⁵G. Jiang, Z. Liu, and J. Hu, *Soft Matter* **9**, 2101704 (2022).
- ¹²⁶L. Cao, A. K. Jones, V. K. Sikka, J. Wu, and D. Gao, *Langmuir* **25**, 12444–12448 (2009).
- ¹²⁷S. Farhadi, M. Farzaneh, and S. A. Kulnich, *Appl. Surf. Sci.* **257**, 6264–6269 (2011).
- ¹²⁸W. Ma, Y. Li, C. Y. H. Chao, C. Y. Tso, B. Huang, W. Li, and S. Yao, *Cell Rep. Phys. Sci.* **2**, 100384 (2021).
- ¹²⁹D. Li, L. Ma, B. Zhang, and S. Chen, *Chem. Eng. J.* **450**, 138429 (2022).
- ¹³⁰Y. Li, W. Ma, Y. S. Kwon, W. Li, S. Yao, and B. Huang, *Adv. Funct. Mater.* **32**(25), 2113297 (2022).
- ¹³¹A. Azimi Yancheshme, A. Allahdini, K. Maghsoudi, R. Jafari, and G. Momen, *J. Energy Storage* **31**, 101638 (2020).
- ¹³²W. Chen, X. Liang, W. Fu, S. Wang, X. Gao, Z. Zhang, and Y. Fang, *ACS Appl. Energy Mater.* **5**, 9109–9117 (2022).
- ¹³³P. Lin, J. Xie, Y. He, X. Lu, W. Li, J. Fang, S. Yan, L. Zhang, X. Sheng, and Y. Chen, *Sol. Energy Mater. Sol. Cells* **206**, 110229 (2020).
- ¹³⁴X. Chen, H. Gao, Z. Tang, W. Dong, A. Li, and G. Wang, *Energy Environ. Sci.* **13**, 4498–4535 (2020).
- ¹³⁵S. Sheng, Z. Zhu, Z. Wang, T. Hao, Z. He, and J. Wang, *Sci. China Mater.* **65**, 1369–1376 (2021).

- ¹³⁶M. Jurkowska and I. Szczygiel, *Appl. Therm. Eng.* **98**, 365–373 (2016).
- ¹³⁷H. Yang, Z. Wang, S. Tan, R. Zang, C. Li, Z. He, J. Meng, S. Wang, and J. Wang, *Adv. Mater. Technol.* **7**, 2200502 (2022).
- ¹³⁸Z. Zhou, Q. Song, B. Huang, S. Feng, and C. Lu, *ACS Nano* **15**, 12405–12417 (2021).
- ¹³⁹Z. He, H. Xie, M. I. Jamil, T. Li, and Q. Zhang, *Adv. Mater. Interfaces* **9**, 2200275 (2022).
- ¹⁴⁰T. Hao, Z. Zhu, H. Yang, Z. He, and J. Wang, *ACS Appl. Mater. Interfaces* **13**, 44948–44955 (2021).
- ¹⁴¹Y. Liu, R. Xu, N. Luo, Y. Liu, Y. Wu, B. Yu, S. Liu, and F. Zhou, *Adv. Mater. Technol.* **6**, 2100371 (2021).
- ¹⁴²Z. Wang, B. Lin, S. Sheng, S. Tan, P. Wang, Y. Tao, Z. Liu, Z. He, and J. Wang, *CCS Chem.* **4**, 104–111 (2022).
- ¹⁴³Y. Yu, B. Jin, M. I. Jamil, D. Cheng, Q. Zhang, X. Zhan, and F. Chen, *ACS Appl. Mater. Interfaces* **11**, 12838–12845 (2019).
- ¹⁴⁴H. Guo, M. Liu, C. Xie, Y. Zhu, X. Sui, C. Wen, Q. Li, W. Zhao, J. Yang, and L. Zhang, *Chem. Eng. J.* **402**, 126161 (2020).